AD-A126 982 MATERIALS RESEARCH FOR ADVANCED INERTIAL INSTRUMENTATION TASK 3: RARE EAR..(U) CHARLES STARK DRAPER LAB INC CAMBRIDGE MA D DAS ET AL. DEC 82 1/1

UNCLASSIFIED CSDL-R-1614 N00014-77-C-0388 F/G 20/3 NL

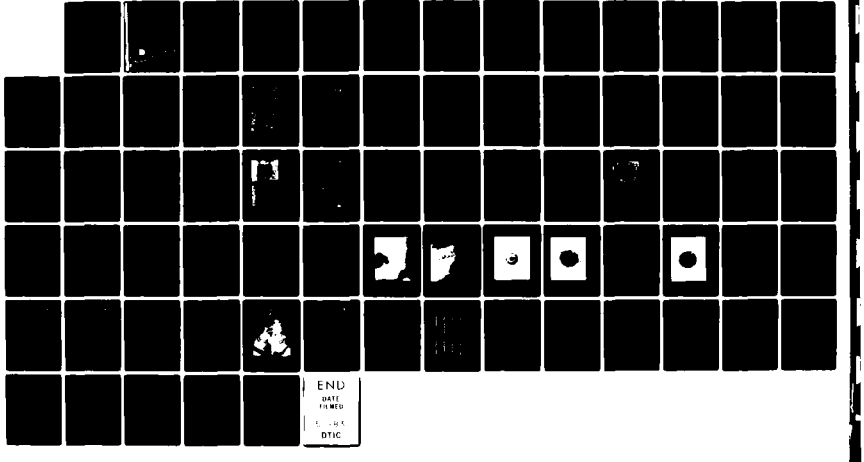

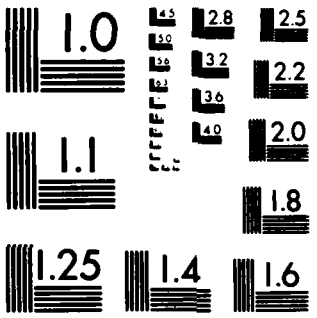

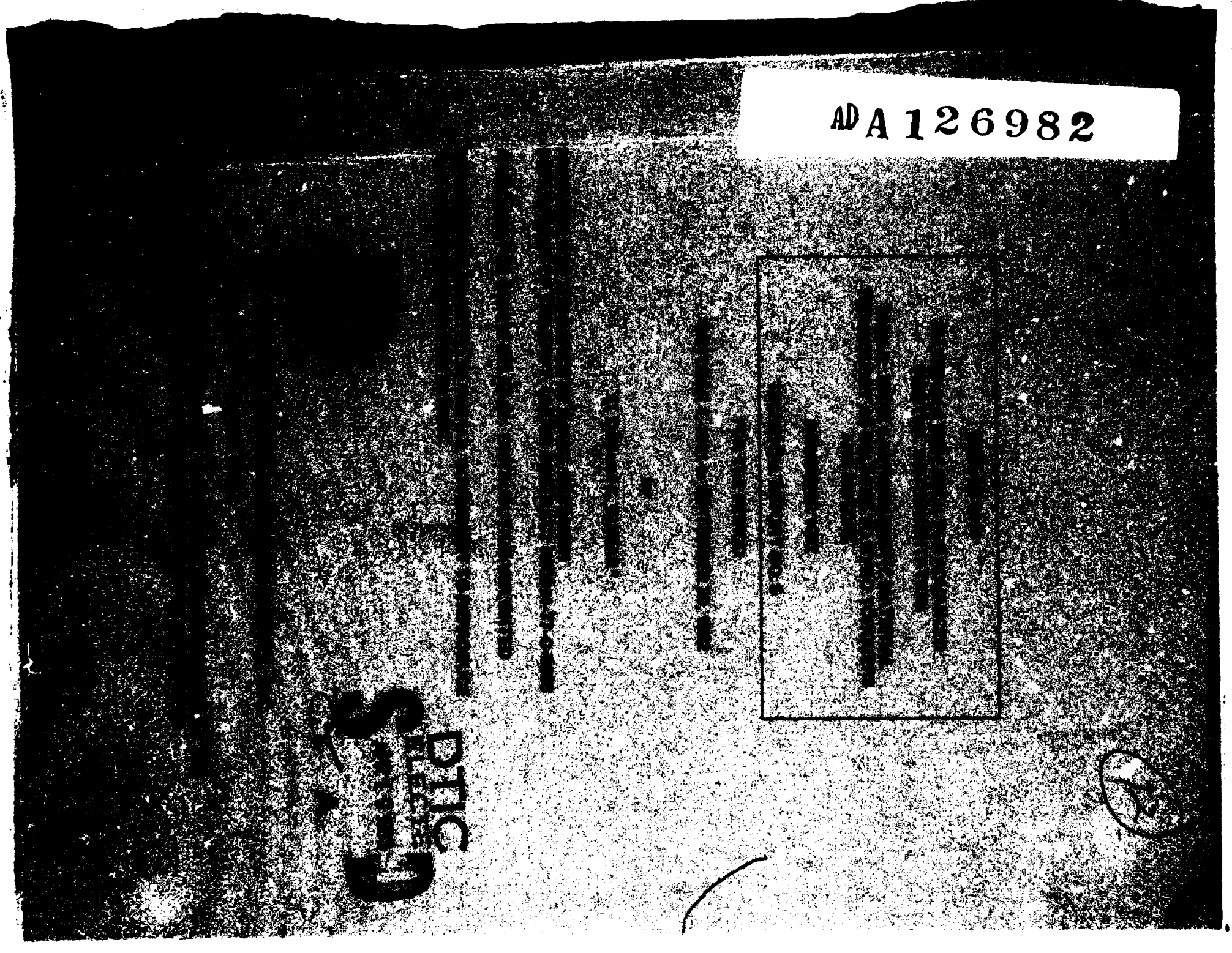

SECURITY CLASSIFICATION OF THIS PAGE *(When Data Entered)*

REPORT DOCUMENTATION PAGE

READ INSTRUCTIONS BEFORE COMPLETING FORM

1. REPORT NUMBER: CSDL-R-1614	2. GOVT ACCESSION NO.: AD-A126 982
3. RECIPIENT'S CATALOG NUMBER:	
4. TITLE *(and Subtitle)*: Task 3: RARE EARTH MAGNETIC MATERIAL TECHNOLOGY AS RELATED TO GYRO TORQUERS AND MOTORS DECEMBER 1982 TECHNICAL REPORT NO. 5 FOR THE PERIOD OCT. 1, 1981 to Sept. 30, 1982	5. TYPE OF REPORT & PERIOD COVERED: Technical Report No. 5 1 Oct. 81 to 30 Sept. 82
	6. PERFORMING ORG. REPORT NUMBER:
7. AUTHOR(s): D. DAS and K. KUMAR	8. CONTRACT OR GRANT NUMBER(s): N00014-77-C-0388
9. PERFORMING ORGANIZATION NAME AND ADDRESS: Charles Stark Draper Labroatory, Inc. Cambridge, Massachusetts 02139	10. PROGRAM ELEMENT, PROJECT, TASK AREA & WORK UNIT NUMBERS:
11. CONTROLLING OFFICE NAME AND ADDRESS: Office of Naval Research Department of the Navy 800 N. Quincy St., Arlington, Virginia 20217	12. REPORT DATE: December 1982
	13. NUMBER OF PAGES: 74
14. MONITORING AGENCY NAME & ADDRESS *(if different from Controlling Office)*: Office of Naval Research Boston Branch, Bldg. 114, Sec. D 666 Summer Street Boston, Massachusetts 02210	15. SECURITY CLASS. *(of this report)*: Unclassified
	15a. DECLASSIFICATION/DOWNGRADING SCHEDULE:

16. DISTRIBUTION STATEMENT *(of this Report)*

Approved for Public Release; distribution unlimited

17. DISTRIBUTION STATEMENT *(of the abstract entered in Block 20, if different from Report)*

18. SUPPLEMENTARY NOTES

19. KEY WORDS *(Continue on reverse side if necessary and identify by block number)*

$SmCo_5$ Magnets	Sintering	Flux Stability
$SmCo_{17}$ Magnets	Temperature Compensated Magnets	
Hot Isostatic Pressing	Thermal Expansion Coefficient	
Arc Plasma Spraying	Permanent Magnets	

20. ABSTRACT *(Continue on reverse side if necessary and identify by block number)*

Flux stability experiments on $SmCo_5$ have demonstrated that no clear correlation or dependence exists between the stability of flux in a magnet and its intrinsic properties H_K and H_{ci}, a belief that has gained wide acceptance on the basis of earlier reported findings. This study shows that the level of the measured flux decay rate is, in contrast, intimately related to the amount of the Sm_2Co_7 phase present in the material (the higher the level, the greater is the decay rate) as well as to the cooling procedure. Fast cooling

7512F 376

DD FORM 1 JAN 73 1473 EDITION OF 1 NOV 65 IS OBSOLETE

SECURITY CLASSIFICATION OF THIS PAGE *(When Data Entered)*

suppresses precipitation of excess oxygen that is present is solid solution at elevated temperatures and this results in a high decay rate at lower operating temperatures. The present results are considered extremely significant in that these provide, it is believed, for the first time the recipe to produce $SmCo_5$ magnets which are very stable with time. The preferred fabrication procedure should include producing of magnets with a composition of near-stoichiometric $SmCo_5$ with a low level of oxygen and possibly a low level of internal stress.

Additional experiments performed with the Er-Sm-Co and Tb-Sm-Co ternary compositions for purposes of producing temperature compensated magnets have resulted in maximum values of $(BH)_{max}$ of 11.6 MGOe and 9.0 MGOe respectively in these two systems. Although these values are substantial improvements over what was previously accomplished, these are still lower than what is believed achievable. Improved alignment procedures are being investigated for this purpose. In regards to the full-circle radial ring $SmCo_5$ magnet that was discussed in the previous annual report, and which can, so far, only be produced with the technology developed under this contract, magnets of specified geometries were fabricated and found extremely useful in application which included a low-cost gyroscope and a travelling wave tube. Superior performance was realized in both instances using this product. A few experiments were also performed, this past year, on the fabrication of low oxygen containing isotropic magnets which were pressed in an inert gas glove box to keep the level of oxygen contamination low. This was achieved, and one magnet thus produced possessed a room temperature H_{ci} value of 56 kOe, believed to be the highest reported for magnets produced by densification of $SmCo_5$ powder. Additional work will concentrate on producing aligned magnets with similar low oxygen levels.

Most of the work performed with the Sm-Co alloys using plasma spraying as the fabrication process concentrated on producing material with crystal anisotropy. A transmission electron microscopic (TEM) examination of a sample that had shown a single sharp crystalline x-ray peak located at the expected peak position for the (00.6) reflection from Sm_2Co_{17}, showed the presence of large (unmelted) 1 to 10μm particles, fine 50 Å grains and amorphous regions. It was concluded that the statistical sampling required for identifying the crystallites, responsible for the (00.6) x-ray peak, would require extensive effort. With respect to producing textured plasma sprayed alloys, the techniques examined included annealing the near-amorphous (time grained and hydrogen treated) materials in the presence of large applied static magnetic fields and thermal gradients, and deposition on substrates maintained at elevated temperatures. Experiments showed that magnetic field annealing did not induce texture in the material. Efforts on temperature gradient annealing also did not yield very encouraging results. These were ambiguous at best. Depositions of $SmCo_5$ compositions at elevated temperatures however, provided for deposits that were highly textured with the c-axis oriented perpendicular to the plane of deposition as indicated by x-ray diffraction patterns obtained on these materials. This is considered a major breakthrough in the fabrication technology of these materials. Plasma spraying is a lower cost process and because of its near-net shape and size capability is expected to find many applications. Further efforts will concentrate on optimizing the composition and heat treatments of the textured deposits for producing high quality $SmCo_5$ magnets.

CSDL-R-1614

MATERIALS RESEARCH FOR ADVANCED INERTIAL INSTRUMENTATION

TASK 3: RARE EARTH MAGNETIC MATERIAL TECHNOLOGY AS RELATED TO GYRO TORQUERS AND MOTORS

DECEMBER 1982

TECHNICAL REPORT NO. 5

FOR THE PERIOD

October 1, 1981 to September 30, 1982

by

D. Das and K. Kumar*

Prepared for the Office of Naval Research
Department of the Navy, under Contract N00014-77-C-0388

Approved:

M.S. Sapuppo, Head
Component Development Department

The Charles Stark Draper Laboratory, Inc.
Cambridge, Massachusetts 02139

* Some of the work described in this report was performed at the Francis Bitter National Magnet Laboratory by the authors as visiting scientists.

ACKNOWLEDGEMENTS

We wish to express our appreciation to the National Magnet Laboratory, MIT, for their assistance by making their high-field magnets available for our studies in this program. Our sincere thanks to C.R. Dauwalter for carrying out the flux stability measurements. The TEM analyses were performed with Professor John B. Van der Sande of M.I.T. serving as the consultant.

This report was prepared by The Charles Stark Draper Laboratory, Inc., under Contract N00014-77-C-0388 with the Office of Naval Research of the Department of the Navy.

Publication of this report does not constitute approval by the U.S. Navy of the findings or conclusions contained herein. It is published for the exchange and stimulation of ideas.

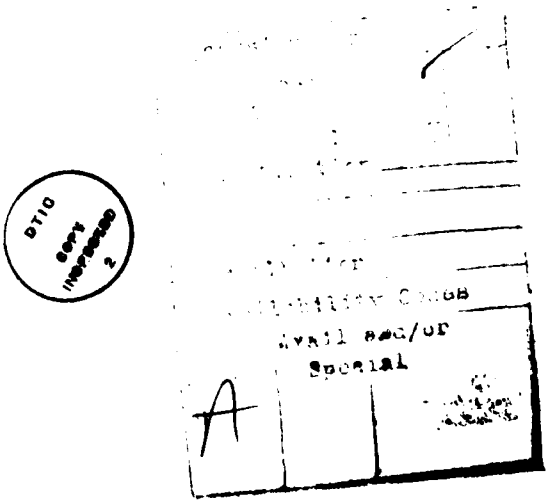

TABLE OF CONTENTS

LIST OF FIGURES

LIST OF FIGURES (continued)

LIST OF TABLES

SECTION 1

INTRODUCTION

1.1 Program Background

The Charles Stark Draper Laboratory, Inc. (CSDL) is involved in research and development in various technologies related to guidance and navigation control for vehicles of all types. Samarium cobalt magnets, because of their high intrinsic coercivity (H_{ci}) and maximum energy product $(BH)_{max}$, are very attractive permanent magnet materials for applications in inertial instruments. They are used within inertial systems as components of the inertial instruments or sensors - the gyro and accelerometer - and as gimbal torque motors. The lower volume of the SmCo magnet impacts favorably on the overall size and weight of the instrument.

In addition to their high energy product, the magnets used in the advanced inertial instruments must also possess long-term flux stability, insensitivity to minor temperature variations, and physical properties compatible with beryllium. (Beryllium is the structural material used in modern inertial instruments.) Commercially available $SmCo_5$ magnets, produced by the state-of-the-art, powder metallurgy process, possess more than adequate H_{ci} and $(BH)_{max}$, and the thermal expansion coefficient requires only a small amount of tailoring to match that of beryllium. The two important areas where the commercial $SmCo_5$ magnets fail to meet the requirements of advanced inertial instruments are: (1) lack of flux stability and (2) large variation of flux associated with a small temperature change.

The Office of Naval Research has sponsored a comprehensive research program at CSDL since October 1977 directed towards improved $SmCo_5$ magnet fabrication procedures to achieve higher flux stability, temperature compensation, and matched thermal expansion with beryllium.

During the first two years of the present program, the efforts focused on sintered and hot isostatically pressed magnets of the $SmCo_5$ composition. A new subtask was added as of October 1979, which concentrates on Sm-Co magnets fabricated by the arc-plasma-spray (APS) process. The motivation behind this subtask was the earlier achievement of outstanding success with near-isotropic $SmCo_5$ magnets using this process at CSDL.

1.2 Objectives

The objectives of the present program are to investigate the arc-plasma-spray process for fabricating improved Sm-Co magnets and to develop improved powder metallurgical procedures to produce inertial-grade $SmCo_5$ magnets which would provide improvements in the following areas:

(1) Long-term flux stability at constant temperature (140°F)

Desired:	0.008 ppm/90-day
Present capability:	Sintered: ~ 1 ppm/day
	Plasma Sprayed: 0.05 ppm/day

(2) Thermal stability of residual induction

Desired:	0.1 ppm/°F
Present capability:	300 ppm/°F

(3) Tailoring of thermal expansion coefficient

Desired, same as beryllium:	6.6 μin./in. ^{0}F
Isotropic:	4.7 μin./in. ^{0}F
Anisotropic:	

(a) Along magnetization direction: 3.1 μin./in. ^{0}F
(b) Normal to magnetization direction: 7.1 μin./in. ^{0}F

SECTION 2

$SmCo_5$ MAGNET INVESTIGATIONS

2.1 Progress Prior to This Report

Four interim annual reports[1,2,3,4]* have been submitted, which describe the progress in this area for a period of four years, from October 1977 to September 1981. The highlights of the past performance are summarized below.

The most challenging of the three objectives, listed in the previous section, was the achievement of a near-zero flux decay rate; the decay rate of the average commercial $SmCo_5$ magnet was found to be about 2000 ppm/decade of days. Since the coercivity of $SmCo_5$ magnets is much higher than that observed in other permanent magnets, the unusually high decay rates shown by these magnets were quite difficult to explain. In contrast, the scientific basis for the other two objectives appeared reasonably clear,[5,6] and thus more easily obtainable. Earlier efforts were therefore directed towards attaining lower decay rates and at the same time gaining an understanding of the mechanisms involved in the unusually high decay rates shown by $SmCo_5$ magnets produced by conventional powder metallurgy processes.

Since the decay of magnetic induction is a demagnetization process, higher stability was expected to demand a greater resistance to such a process. In turn, this meant that both the intrinsic coercivity H_{ci} and H_k (reverse field at 90 percent $4\pi M_R$) had to be improved substantially over the state-of-the-art magnets which have H_{ci} in the range of 20 to 30 kOe and H_k of 5 to 10 kOe, notwithstanding the fact that these values were already an order of magnitude higher than those of the other permanent magnets known at the time. In order to achieve

*Superscripted numerals refer to sources in the List of References.

this difficult goal the $SmCo_5$ magnet fabrication technique had to be improved to produce contamination-free magnets, particularly oxygen, with fine grain size. The standard sinter technology was therefore improved significantly, and this resulted in magnets with outstanding intrinsic coercivity: H_{ci} of approximately 50 kOe and H_k of 33.5 kOe. This resulted in an improvement in the flux decay rate to 280 ppm/decade. In a parallel effort, the hot isostatic pressing (HIP) technique was developed for producing $SmCo_5$ magnets, which resulted in magnets with properties comparable to sintered magnets. The oxygen content of these magnets was about half of what is found in sintered magnets. Initial HIPed $SmCo_5$ magnets showed an improved low decay rate of 160 ppm/decade. More recent studies of flux decay rates have shown that the amount of the second phase Sm_2Co_7 present in the magnet plays a much more significant role. Larger amounts of the second phase produced a higher rate of decay. Preliminary measurements of flux decay rates of high coercivity and high energy product HIPed $SmCo_5$ magnets had shown that the decay rate increased from 43 ppm/decade to 1070 ppm/decade when the samarium content was increased by one weight percent.

At the beginning of the third year, experimental work was initiated on the temperature compensated magnets as well as thermal expansion measurements (with the above-stated objectives of producing temperature stability and matching the expansion coefficient of the magnet with that of beryllium) in addition to the continued efforts on the study of flux stability. Initial sinter experiments were performed to determine the compositions necessary to obtain zero temperature coefficients using $ErCo_5$ and $TbCo_5$ to replace part of $SmCo_5$. Larger percentages of these compounds were found to be necessary to obtain zero temperature coefficient than what was expected to be required on the basis of published data. As a result, the B_r values were much lower than previously estimated. In addition, there was some loss of the potential B_r because of poor alignment obtained by die pressing and sintering. The situation was somewhat alleviated by pursuing HIP processing instead of the conventional sinter technique. Initial HIPed magnets gave higher B_r values but lacked the necessary coercivity.

However, based on the higher B_r values, the potential of higher energy product was seen if the coercivity could be improved by increasing the overall rare earth to cobalt ratio.

The highest energy product CSDL $SmCo_5$ magnets, prepared by HIP (21 MGOe) and die-pressed sintered (18 MGOe) were found to have two percent higher and two percent lower thermal expansion coefficients, respectively, than that of beryllium. Obviously an $SmCo_5$ magnet with an energy product of between 19 and 20 MGOe would give a very satisfactory match with beryllium for thermal expansion compatibility, which would require little if any further effort.

Radially oriented full-circle $SmCo_5$ ring magnets have been impossible to produce by sinter technology, although many applications require such magnets. Using the HIP technique developed for $SmCo_5$ magnets at CSDL, ring magnets with radial orientation of high magnetic properties and well controlled geometry were produced. These were expected to play an important role in the magnetic circuitry of torque generators in inertial instruments.

2.2 Progress during This Reporting Period

2.2.1 Further Studies on Flux Stability

Based on the findings prior to the present reporting period, it appeared that there were two distinct mechanisms which were responsible for the unexpectedly high decay rates seen in $SmCo_5$ magnets:

(1) Presence of Sm_2Co_7 in the fabricated magnet which is deliberately added to the alloy composition to promote the sintering characteristics

(2) Formation of Sm_2Co_{17} caused by the precipitation of dissolved oxygen in the $SmCo_5$ lattice

The first of these two conclusions was arrived at on the basis of a rather limited amount of experimental data on just two sets of samples prepared by the HIP technique. Further verification was considered necessary on not just HIPed magnets but also on the sintered type. Therefore, it was decided that sintered $SmCo_5$ magnets with three different compositions would be tested for flux stability. The compositions selected were 35.0, 35.5, and 36.0 percent samarium. The compositions of stoichiometric $SmCo_5$ and Sm_2Co_7 are 33.8 and 42.2 percent samarium, respectively. The three compositions selected would contain appreciably different amounts of the second phase Sm_2Co_7 to reveal the variation of flux decay rate as a function of the Sm_2Co_7 content.

The startup alloy powders of the selected compositions were prepared by blending sinter grade powders of 34.5 percent samarium and 42 percent samarium alloys in calculated proportions. Disc-shaped compacts were produced from these powder mixtures in an aligning magnetic field of about 15 kOe under a compaction pressure of 50 kpsi. The green compacts were sintered at 1125°C for 3 hours followed by aging at 900°C for 24 hours in a high purity helium atmosphere. Some of the samples of each composition were quick cooled and others were furnace cooled following the 900°C aging. The samples of each category were then subjected to the following evaluation procedures:

(1) Magnetic measurement to determine B-H characteristics

(2) Metallographic examination to determine phase composition, homogeneity, grain size, porosity, etc.

(3) Oxygen analysis

The results of magnetic measurements are given in Table 1 for both the quick cooled and the furnace cooled samples. Typical microstructures of the magnets are shown in Figures 1, 2, and 3. Table 2 shows the oxygen content of the magnets.

Table 1. Magnetic properties of flux stability magnets with samarium content of 35.0, 35.5 and 36.5 percent. Sintered at 1120°C - 3 hours, 900°C - 24 hours.

Composition % Samarium	Cooling after Heat Treatment	B_r (KG)	H_{ci} (kOe)	H_c (kOe)	H_k (kOe)	$(BH)_{max}$ (MGOe)
35.0	Quick cooled	6.7	34.0	6.3	12.4	10.6
35.5	Quick cooled	7.1	47.0	6.9	15.4	12.2
36.0	Quick cooled	7.1	48.0	7.1	10.5	12.6
35.0	Furnace cooled	6.6	2.0	-	-	-
35.5	Furnace cooled	7.3	31.0	6.0	4.0	11.6
36.0	Furnace cooled	7.1	37.5	6.2	5.4	9.9

Table 2. Oxygen analyses of flux stability magnets.

Sample	Oxygen %
35.0	0.445
35.5	0.493
36.0	0.424

Figure 1. Etched microstructure of 35.5% Sm alloy magnet; quick cooled after 900°C aging. 500X.

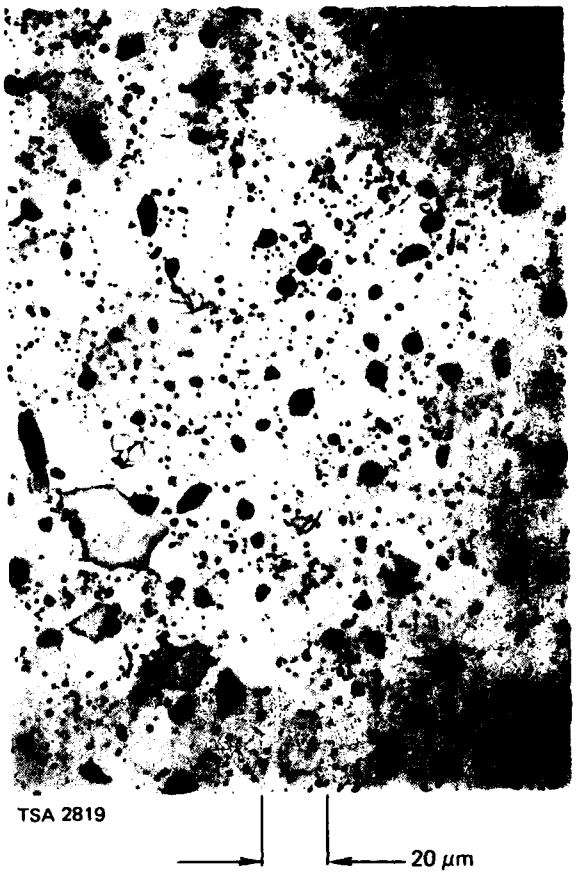

Figure 2. Etched microstructure of 35.5% Sm alloy magnet; quick cooled after 900°C aging. 500X.

Figure 3. Etched microstructure of 36.0% Sm alloy magnet; quick cooled after 900°C aging. 500X.

Magnetic property measurements brought out the fact that 35.5 and 36.0 percent samarium retained fairly high coercivities on furnace cooling, but the 35.0 percent samarium magnets could not retain enough coercivity for flux stability measurements. All the samples had good coercivity in quick cooled conditions and would therefore be suitable for stability measurements. Although the magnets become more stable when furnace cooled, we had to settle for quick cooled conditions in order to be able to compare the stabilities of all three compositions. On the basis of the compositions the 35.0, 35.5 and 36.0 percent samarium alloys should contain 15, 21 and 28 percent Sm_2Co_7, respectively. But because of about 0.4 percent oxygen content the Sm_2Co_7 contents are much less, since all the oxygen in excess of the amount that is dissolved in the $SmCo_5$ lattice forms Sm_2O_3, reducing the amount of samarium available for the alloy. Microstructure examination clearly showed increasing amounts of Sm_2Co_7 based on increased amounts of samarium in the magnets, but clearly much less than the calculated amounts. The micrographs also reveal that the porosity in the 35.0 percent magnet is much higher, indicating that the higher amount of samarium, as in the other two alloys, is necessary to obtain better sinterability. The lower B_r value of the 35.0 percent alloy is directly related to lower sintered density. The B_r values of all the magnets are rather low, indicating that die pressing and sintering do not usually produce good particle alignment. Nevertheless, the magnetic properties were sufficiently high to let us proceed to the next step, viz the measurements of decay rate.

As described in earlier reports, the flux decay rate measurement apparatus requires 12 rectangular magnet samples of an identical geometry. The machined samples are given the final heat treatment, magnetized and mounted in a Carpenter-49 alloy cylinder by bonding with epoxy at 150°C for 16 hours. The mounted samples are then introduced into a torque generator circuit and rotated at a constant speed while being maintained at a constant temperature of about 140°F during the entire measurement period. A voltage is generated in the pickup coils. The decline of the voltage with time is a direct measure of the magnetic flux decay rate.

The above procedures were used to measure the flux decay rates of one set each of 35.5 and 36.0 percent samarium magnets and two sets of the 35.0 percent samarium batch. The selection of sample composition was based on the expectation that the results would demonstrate the dependence of flux stability as a function of the amount of the second-phase Sm_2Co_7. That is, the larger amounts of Sm_2Co_7 in the alloys would produce larger decay rates. Duplicate runs of the 35.0 percent samples were performed to determine whether the chosen method of flux decay measurement does indeed produce dependable results. The results of these measurements, as will be seen later, have shown that our expectations were correct and have also demonstrated that the measurement data of the present apparatus are reasonably dependable.

The results of the measurements were plotted on semi-log graph papers, with time on the log scale versus the decay of flux. It was demonstrated in earlier reports that a reasonably straight line relationship between flux decay and log time could be obtained if the zero time were assumed to be the end of the last heat treatment. Figures 4 and 5 show the decay rate plots of the two batches of 35.0 percent samarium magnets and Figures 6 and 7 are those of the 35.5 and 36.0 percent samarium magnets. Unfortunately, there were some delays and interruptions in the measurements of these samples. In the case of the 35.5 and 36.0 percent samarium magnets, more than two months had elapsed, since the last heat treatment and magnetization of the samples, before the flux decay measurements commenced. The two sets of 35.0 percent samarium magnets encountered an interruption in measurements for 35 days at the end of 47 days of initial measurements. The samples were maintained at the measurement temperature during the interruption period. Measurements were then resumed and continued for another 50 days. The decay rates for the samples were determined from Figures 4 through 7 and recorded in Table 3.

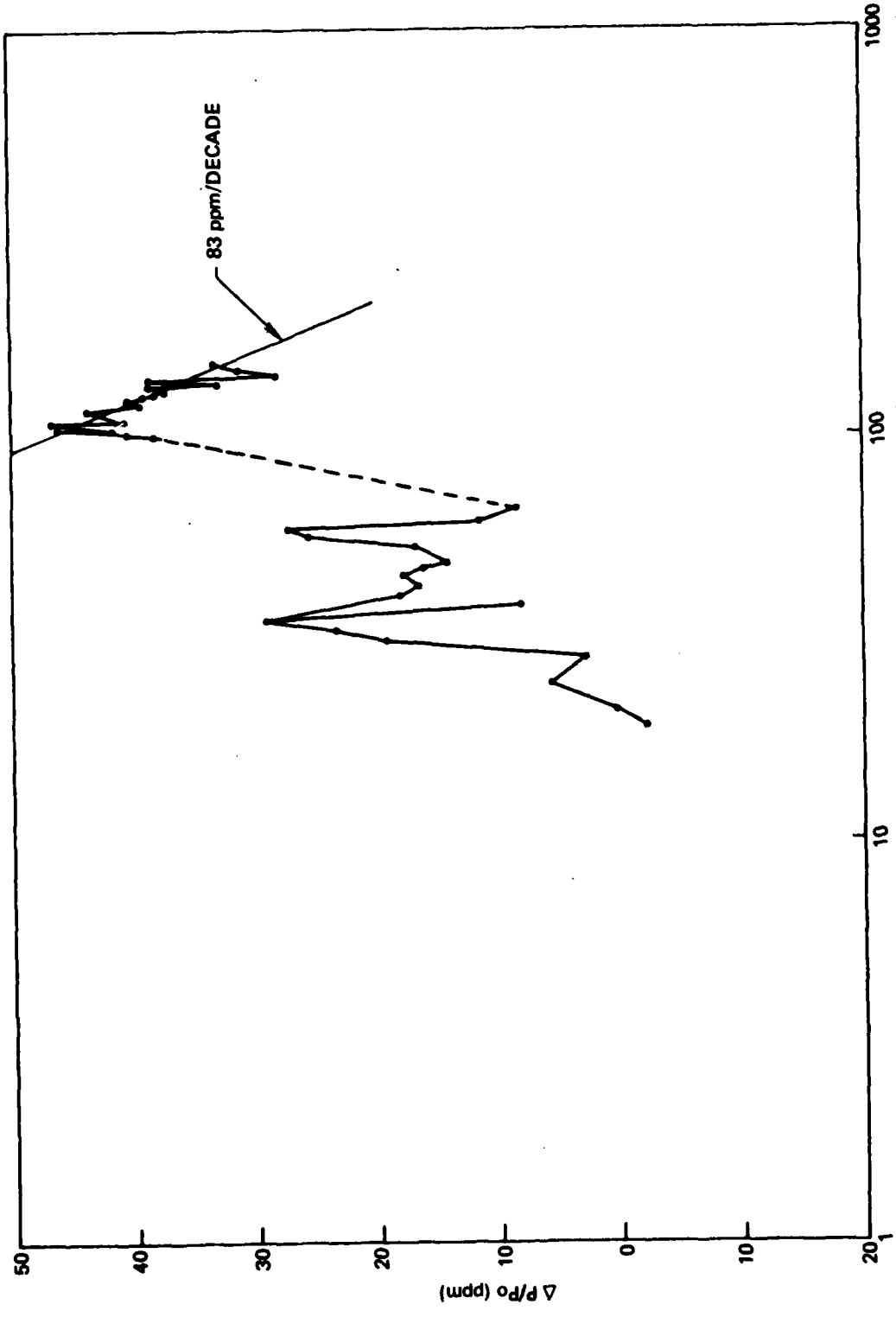

Figure 4. Flux decay vs. log time for magnets 35.0% Sm.

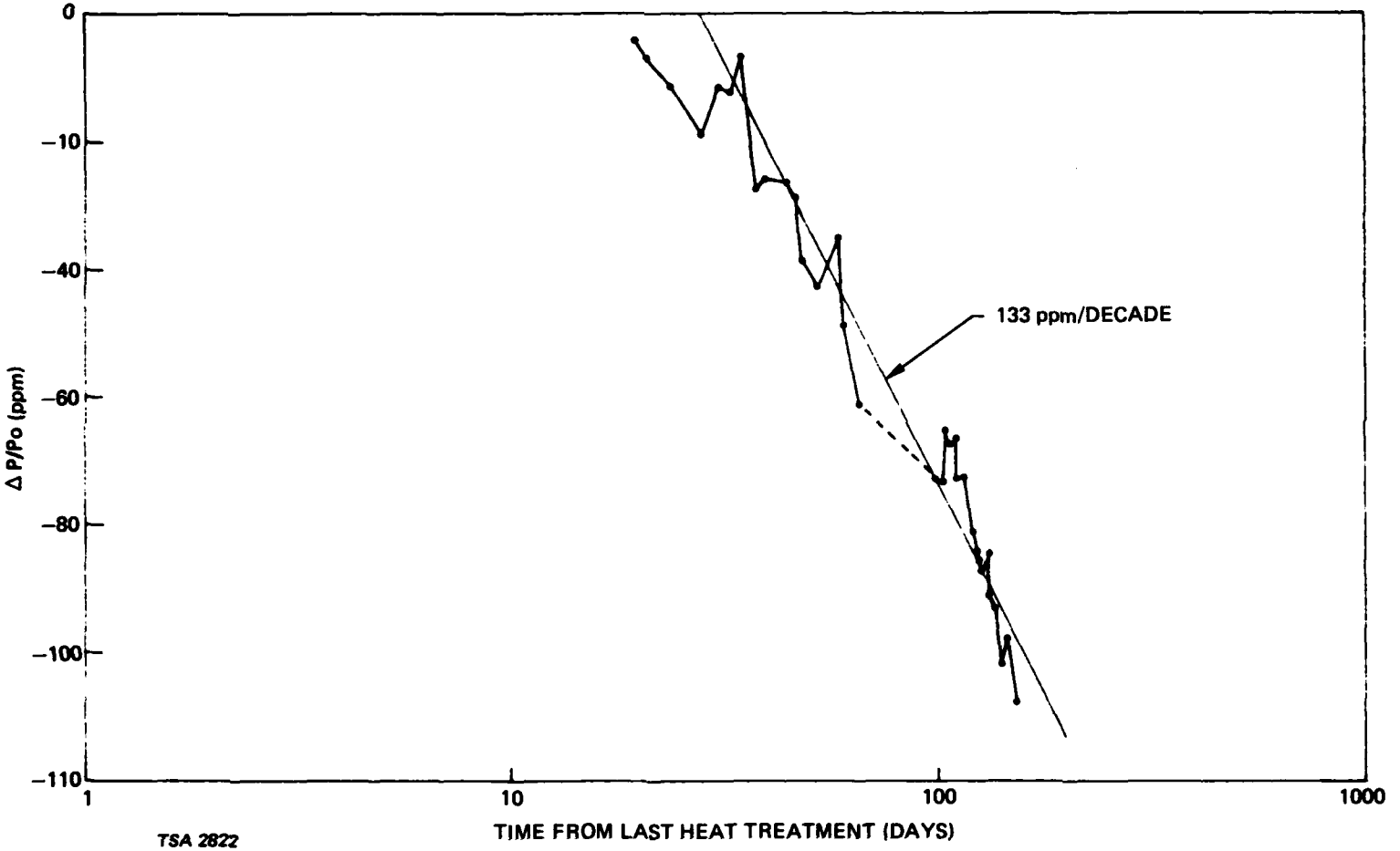

Figure 5. Flux decay vs. log time for magnets 35.0% Sm, No. 2.

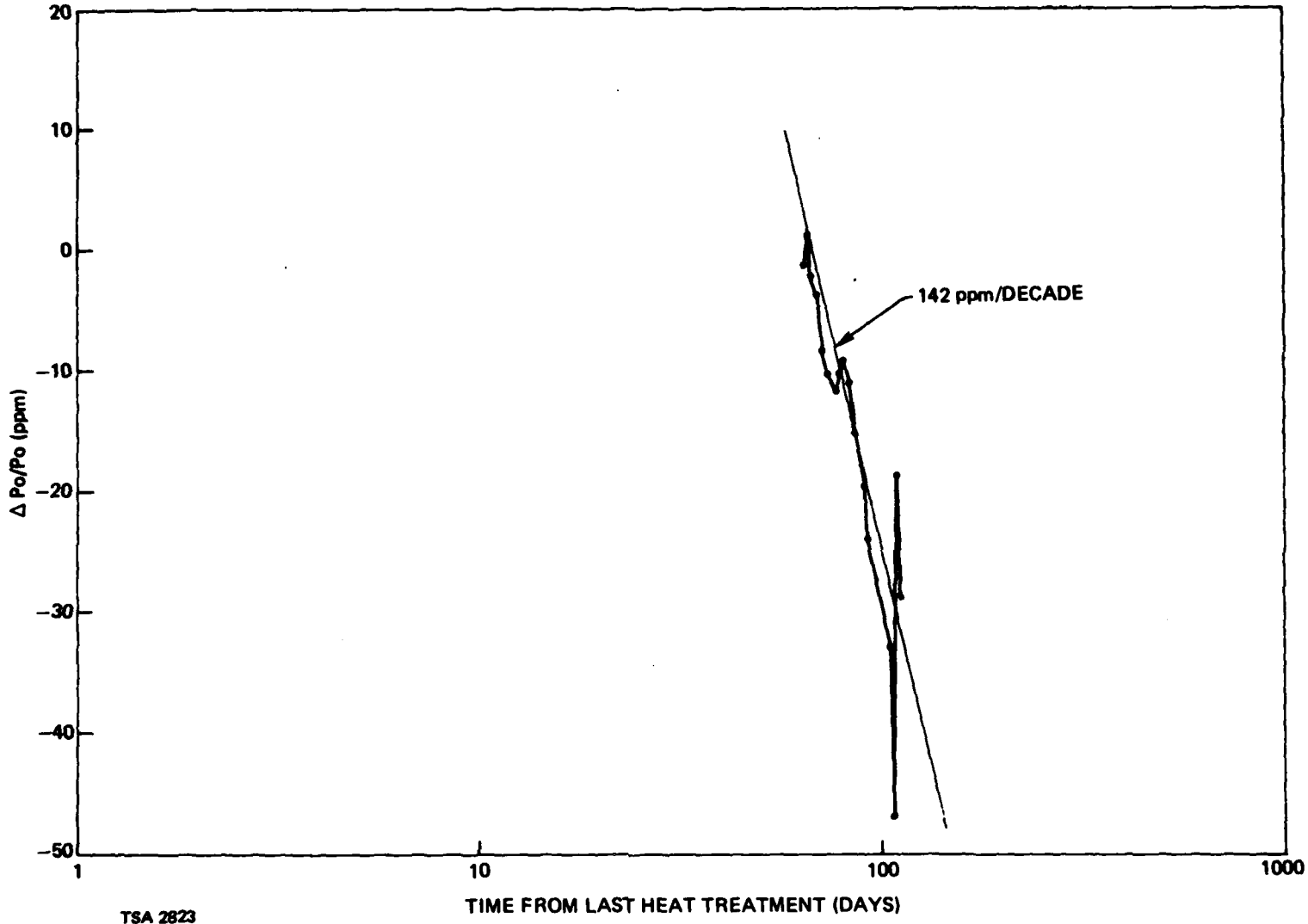

Figure 6. Flux decay vs. log time for magnets 35.5% Sm.

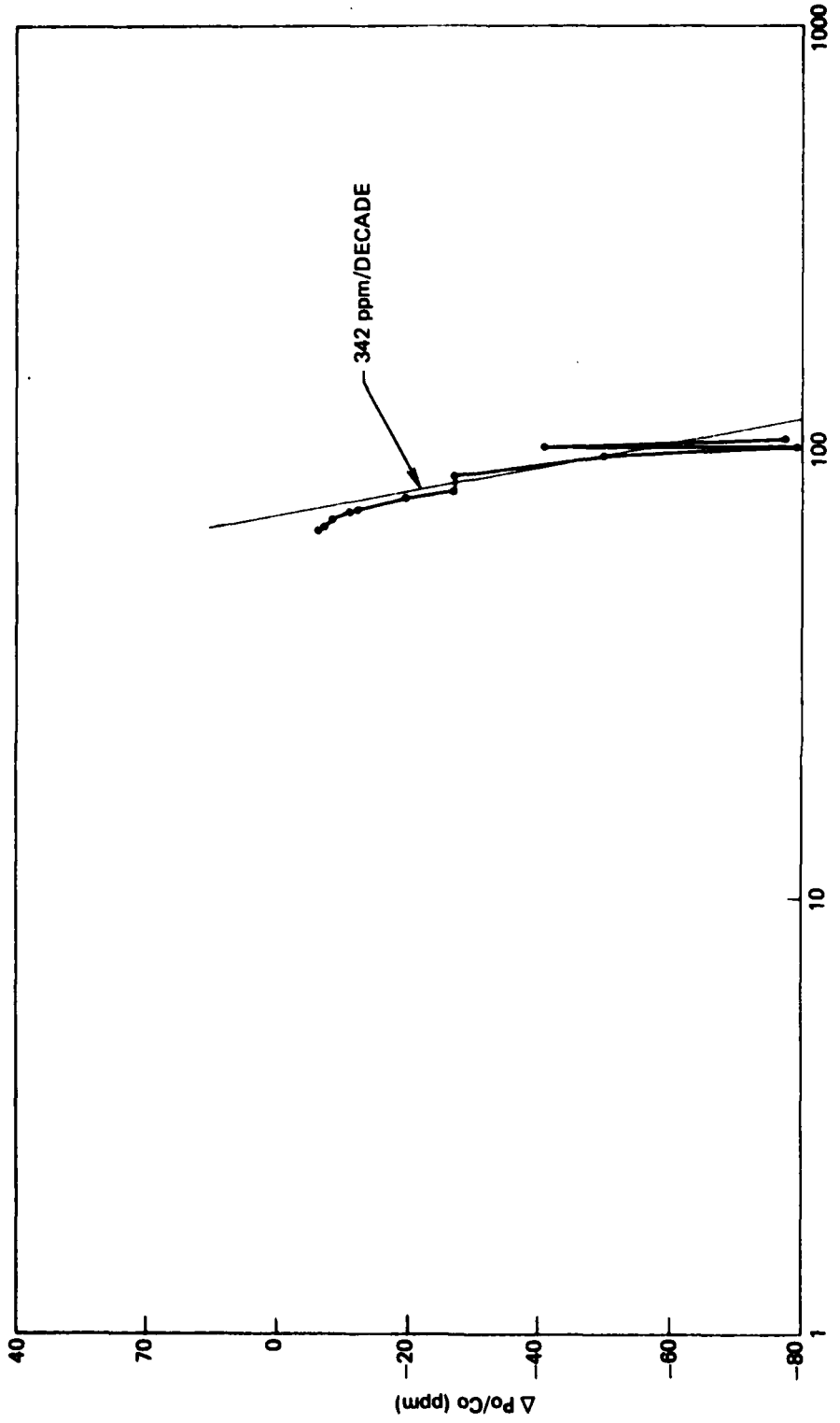

Figure 7. Flux decay vs. log time for magnets 36.0% Sm.

Table 3. Measured flux decay rates of 35.0, 35.5 and 36.0 percent samarium magnets, which were quick cooled from 900°C aging.

Sample No., Percent Sm	Fabrication Process	Coercivities		Decay rate ppm/decade of days
		H_{ci}(kOe)	H_K(kOe)	
35.0 No.1	Sintered	34.0	12.4	83
35.0 No.2	Sintered	34.0	12.4	133
35.5	Sintered	47.0	15.4	142
36.0	Sintered	48.0	10.5	342
24-36.5*	Sintered	44.0	33.5	761

* From report No. 3 of this program.

The results presented in Table 3 show that as the samarium content of the magnet is increased from 35 to 36 percent, thereby increasing the amount of the second phase Sm_2Co_7 (see Figures 1, 2, and 3), the flux decay rates increase monotonically from a low of 83 ppm/decade to 342 ppm/decade. As previously reported,[3] a magnet sample with 36.5 percent samarium, fabricated in a similar manner as the present samples and subjected to similar thermal treatment of quick cooling from the 900°C aging treatment, gave a decay rate of 761 ppm/decade. (The latter sample had an H_{ci} of 44 kOe and H_k of 33 kOe, and the data are reproduced in Table 3.) The decay data of Table 3 are shown graphically as curve No. 1 in Figure 8.

The 36.5 percent samarium flux stability samples were restored to their high temperature homogenized condition by heat treating and then furnace cooled after the 900°C aging. Flux stability measurements were reported on some HIPed magnet composites in last year's report. These were also furnace cooled after aging. The measured magnetic properties and the decay rate measurement on the earlier magnets, which have already been recorded in previous reports, are shown in Table 4.

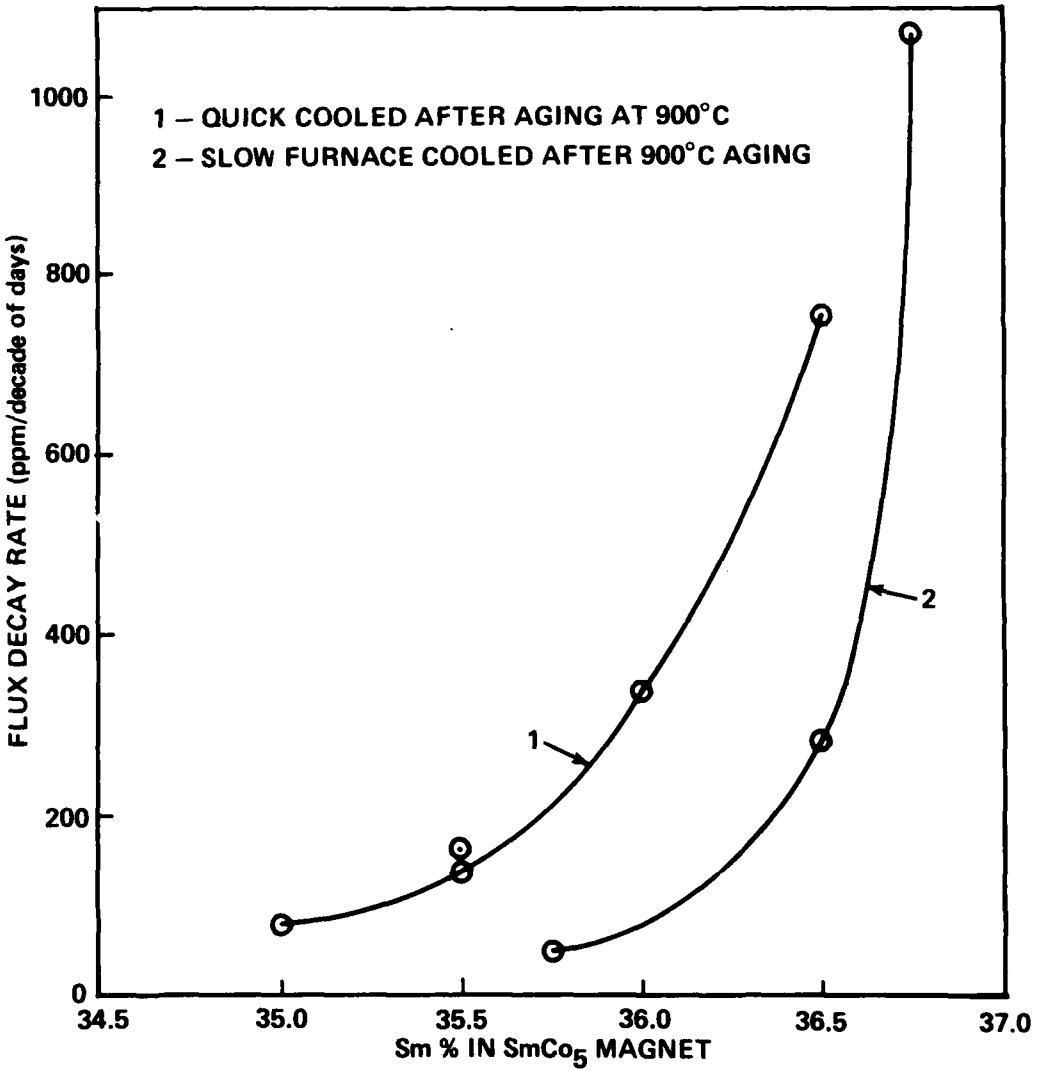

Figure 8. Flux decay rates of $SmCo_5$ magnets as a function of Sm content and thermal treatment.

Table 4. Flux decay rates and magnetic properties of some slow cooled samples after 900°C aging.

Sample No.	% Sm	Fabrication Process	Coercivities		Decay rate ppm/decade of days
			H_{ci}(kOe)	H_K(kOe)	
24	36.5	Sintered	23	19.0	280
H-26 + H-27	35.75	HIPed	22	7.5	43
H-28 + H-29	36.75	HIPed	30	8.0	1070

The decay data of Table 4 have also been plotted in Figure 8 as curve No. 2. Both curves 1 and 2 are decay rates of $SmCo_5$ magnets as a function of composition; however, the curve No. 2 magnets show lower decay rates than those of No. 1 for the same composition. The curve 1 magnets were quick cooled from the aging temperature, whereas the others were cooled slowly inside the furnace. It has been shown in previous reports that the slow cooling process from aging temperature generally lowers the coercivity values. It was adequately explained that it does so by precipitation of excess dissolved oxygen from the $SmCo_5$ lattice and causing formation of some Sm_2Co_{17} phase. Although the coercivity is lowered, the flux stability instead of degrading actually improves significantly.

Until the present studies in flux stability it was generally accepted[6] that the higher the coercivity of the $SmCo_5$ magnets, particularly the H_k value, the higher the expected stability of magnet flux. This study clearly shows that coercivity plays a minor role in the flux decay process. The following conclusions about stability of $SmCo_5$ magnets can now be drawn based on the experimental results that have been obtained.

(1) In contrast to earlier findings, the value of H_k has little bearing on the flux decay rate.

(2) At least two mechanisms appear to be responsible for the observed flux decay rates:

(a) The presence and respective amounts of the Sm_2Co_7 phase. The larger the amount, the higher the decay rate.

(b) Lowering of dissolved oxygen (and perhaps internal stress to a lesser extent) by slow cooling from aging temperature lowers the decay rate.

(3) To maximize stability of magnet flux the material should be composed of near-stoichiometric $SmCo_5$ with low oxygen and possibly a low internal stress.

It will be very desirable to produce a few more data points for both the curves of Figure 8. This can be easily accomplished by either slow cooling some of the samples of curve No. 1 and fast cooling some of the samples of curve No. 2. Some more samples should be studied with even lower samarium content than the lowest (35.0 percent) studied so far. This can be done only by HIP, since nearly the lowest limit of composition for sintering had been reached. In addition to the ability of HIP to densify SmCo alloy powders with less than 35.0 percent samarium, the powder particle size can be substantially larger, which would result in lowered oxygen content. As was already stated, it would be very desirable to lower the oxygen content of the finished magnet in order to achieve higher stability.

2.2.2 Temperature Compensated Magnets

Inertial instruments are usually operated at a constant temperature somewhere in the range of 130° to 160°F. It is desirable that the $SmCo_5$ magnets used in the sensor circuitry possess a near-zero temperature coefficient in this range of temperature. Recent measurements at CSDL on high energy product magnets prepared in the laboratory have shown that the temperature coefficient of magnetization is about 180 ppm/°F variation in temperature in the temperature range of 130° to 160°F.

In contrast to the normal negative temperature coefficient for $SmCo_5$, the heavy rare earth (HRE)-cobalt compounds show positive temperature coefficients of larger magnitude than that of $SmCo_5$ in the desired temperature range. Calculations based on available data had shown that the magnets of compositions (66.7% $SmCo_5$ + 33.3% $ErCo_5$) and (81.8% $SmCo_5$ + 18.2% $TbCo_5$) should have a near-zero temperature coefficient at gyro operating temperatures. The corresponding expected $(BH)_{max}$ values would be 17.2 and 18.7 MGOe, respectively, at 100 percent density and alignment and 15.5 and 16.8 MGOe at 90 percent alignment.

Our initial temperature compensated magnets, produced by die-pressing and sintering, showed that a zero temperature coefficient could be obtained in $SmCo_5$ magnets by replacing about 40 percent of the $SmCo_5$ by either $ErCo_5$ or $TbCo_5$. Because of poor alignment in die pressing, the energy products were only about 7 and 5.5 MGOe, respectively. Various compositions of the above two binary systems were then fabricated by cold isostatic pressing of aligned powder and HIPing the resulting green compacts. These samples showed higher B_r values, indicating the potential for higher energy products. However, the coercivities were much too low to bring about the improvement in energy product. Temperature coefficient measurements revealed that the zero coefficient composition for the $ErCo_5$ + $SmCo_5$ system was slightly higher than 35 percent $ErCo_5$ but less than 40 percent. In the case of $TbCo_5$, the zero composition was found to be between 30 and 35 percent $TbCo_5$. Microstructure of the samples showed the presence of an RE_2Co_{17} phase, which would account for the poor coercivities. Obviously, then, the percentage of the rare earth had to be increased, which could be accomplished by adding an additional amount of Sm_2Co_7 powder to the alloy powder mixtures. This was done and four more HIPed magnet ingots were fabricated with the following compositions: 30% $TbCo_5$ + 70% $SmCo_5$, 35% $TbCo_5$ + 65% $SmCo_5$, 35% $ErCo_5$ + 65% $SmCo_5$, and 40% $ErCo_5$ + 60% $SmCo_5$. A large number of 0.5-inch-diameter x0.2-inch-thick discs were removed from each of the HIP ingots for various heat treatments as follows: 1050°C - 24 hours, 1075°C - 24 hours, 1100°C - 24 hours, 1120°C - 3 hours, 1140°C - 3 hours, 1160°C - 3 hours, and 1180°C -

3 hours. Following each of these heat treatments, the samples were cooled down to 900°C and held for 24 hours and quick cooled. Intrinsic magnetic properties were measured in each case. In as-HIPed condition all samples had poor coercivities. However, except for sample E-40, the other three showed substantial improvement after various heat treatments. Typical microstructures of 1160°C treated samples, etched to reveal the second phase or phases, are shown *in Figures* 9, 10, 11, and 12. The terbium-containing samples show well dispersed Sm_2Co_7 particles, which is a situation conducive to producing high coercivity. Both of the erbium-containing samples show Sm_2Co_{17} phase, known to damage the coercivity of $SmCo_5$-type magnets. The amount of Sm_2Co_{17} in the E-35 samples is rather small and therefore the coercivity is not so badly damaged. However, E-40 shows excessive amounts of Sm_2Co_{17} and the result is poor coercivity in these samples. The best magnetic properties of these magnets were attained at different heat treatments. The results are presented in Table 5.

With reference to the samples T-30 and E-35, the achieved energy products of 9.0 and 11.6 MGOe are rather low compared to the theoretical maximum values of 14.1 and 17.0 MGOe and values of 12.6 and 15.3 MGOe, respectively, expected at 90 percent alignment. A very strong suspicion at this time is that the alignment during compaction was poor. Therefore, efforts should go into achieving better alignment. On the other hand, an energy product of 11.6 MGOe may be acceptable if the other requirements, such as time dependent flux stability and thermal expansion characteristics, are satisfactory. Investigations on these other properties are now in progress on both the erbium- and terbium-containing temperature compensated magnets, and will be reported in due course.

Figure 9. Typical microstructure of T-30, after 1160°C heat treatment. 3% Nital etch. 500X.

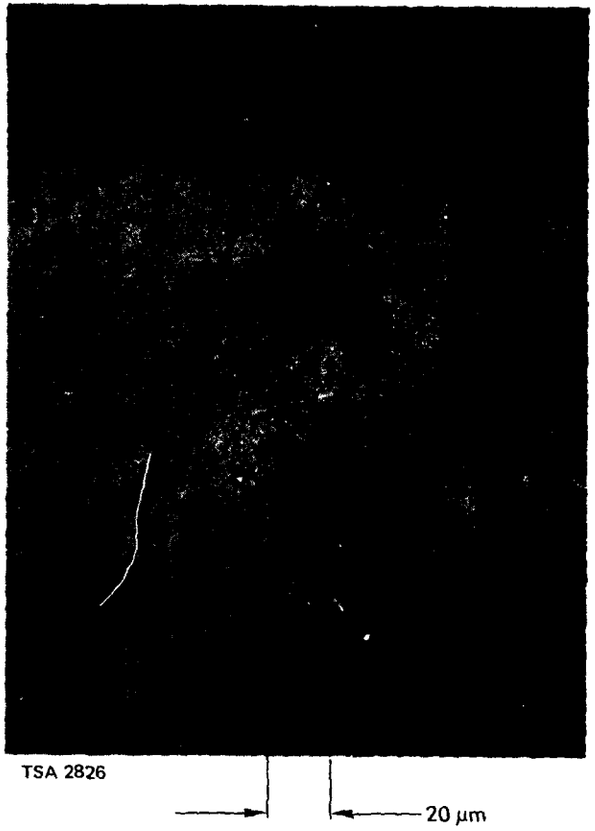

Figure 10. Typical microstructure of T-35, after 1160°C heat treatment. 3% Nital etch. 500X.

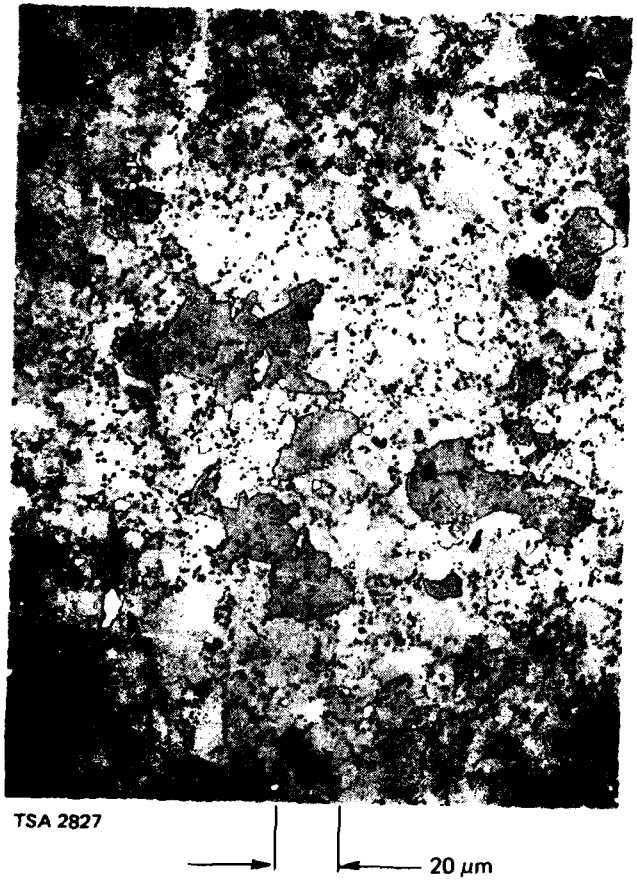

Figure 11. Typical microstructure of E-35, after 1160°C heat treatment. 3% Nital etch. 500X.

Figure 12. Typical microstructure of E-40, after 1160°C heat treatment. 3% Nital etch. 500X.

Table 5. Best values of magnetic properties of temperature compensated magnets, and the corresponding heat treatment after hot isostatic pressing.

Sample	Heat Treatment	(B_rkG)	H_{ci}(kOe)	H_c(kOe)	H_k(kOe)	$(BH)_{max}$(MGOe)
T-30	1180°C-3 hrs, 900°C-24 hrs, Q.C.*	6.0	15.0	5.8	9.4	9.0
T-35	1180°C-3 hrs, 900°C-24 hrs, Q.C.	5.3	29.0	4.8	4.3	6.8
E-35	1160°C-3 hrs, 900°C-24 hrs, Q.C.	6.9	15.0	6.5	9.5	11.6
E-40	1120°C-3 hrs, 900°C-24 hrs, Q.C.	6.5	4.5	---	---	----

* Q.C. - quick-cooled following 900°C treatment

From the studies carried out thus far on the two ternary systems, Er-Sm-Co and Tb-Sm-Co, the following observations are drawn:

(1) Near-zero temperature coefficients occur in Er-Sm-Co and Tb-Sm-Co magnets at the compositions of slightly higher than 35 percent $ErCo_5$ and slightly lower than 35 percent $TbCo_5$.

(2) The maximum energy products achieved are 9.0 MGOe for Tb-Sm-Co and 11.6 MGOe for Er-Sm-Co magnets as compared to 12.6 and 15.3 MGOe, respectively, that are believed achievable.

(3) Better alignment may produce the higher energy products indicated in (2), and investigations are now in progress to determine if this can be accomplished.

2.2.3 Radial Ring Magnets by HIP

Last year it was reported that a significant milestone was achieved in the HIP processing of $SmCo_5$ magnets. Using this technology, newly developed at CSDL, full-circle radially oriented $SmCo_5$ ring magnets were successfully produced with high intrinsic magnetic properties. Until that time, successful fabrication of radial ring magnets had eluded all attempts. During the past year, radial ring magnets of specified geometries have been fabricated for the following applications:

(1) Torque generator of a CSDL-designed low-cost gyroscope

(2) Electron beam focusing within a slow wave structure of a traveling wave tube.

Superior performance, as expected from magnets with radial orientation, have been realized in both of the above applications. The fabrication of these magnets was carried out under independent funding.

It is believed that the radially oriented $SmCo_5$ magnets will eventually be used in many significant applications, where they will perform in a more superior manner than the unidirectionally oriented magnets that are currently available. There are some minor problems associated with the mechanical integrity of the radial magnets which, however, do not deter their usage. Nevertheless, a research and development effort should be directed towards the elimination of the problem. It may be possible to accomplish this if funds become available.

2.2.4 Low-Oxygen $SmCo_5$ Magnets

Oxygen plays a damaging role on the flux stability of $SmCo_5$ magnets (and perhaps also on the coercivities). Because of the inherent affinity of samarium for oxygen, the conventional die-pressed and sintered magnets contain about one-half percent oxygen at the minimum and sometimes as much as one percent. Practically all of this oxygen enters the $SmCo_5$ magnets from surface contamination of the powder particles of the alloy, as a consequence of powder preparation and handling in an air atmosphere. In order to avoid oxygen pickup by the $SmCo_5$ powder, a special chamber was built to carry out powder preparation, drying of the powder, compaction and encapsulation of the powder compact inside HIP cannisters in an oxygen-free argon atmosphere. The chamber was designed and built with funds provided under a related magnet program.

For the initial experiments, two commercial Sm-Co alloys with 34.5 and 41.8 percent samarium were used as the starting materials. The alloys were crushed in a jaw crusher followed by pulverizing in a double-disc pulverizer. The disc-ground powder was sieved through a 100-mesh screen and the +100-mesh fractions were used for subsequent processing in the comminution chamber. All of the above processing steps were carried out in air atmosphere and the oxygen contamination at that stage was only about 0.034 percent. Calculated amounts of the two alloys were blended to produce 35.5 percent and 36.0 percent samarium

mixtures. These mixtures, in 100-gram batches, were ground in an attritor ball mill for 15 minutes and two hours respectively inside the chamber and taken through the rest of the processing to end up in welded HIP cannisters before being brought out from the chamber for HIP. The 15-minute attritor grinding produces a powder size of 5 to 10 μm used for normal $SmCo_5$ HIP procedures. The two-hour grinding was expected to produce a much finer particle size. The samples were HIPed at 950°C for 2 hours at 15 kpsi. They were subsequently removed from the HIP cans and sliced to produce B-H curve measurement samples. B-H measurements were carried out on samples in as-HIPed condition as well as after selected heat treatments. Oxygen analyses were performed on the starting +100-mesh powders and the HIPed samples. Microstructures were examined on the HIPed samples to determine the presence and identity of second-phase particles as well as grain size in the magnets. The results of oxygen analysis are shown in Table 6 and some selected microstructures are shown in Figures 13 through 16. The coercivities of the various samples are shown in Table 7.

Table 6. Oxygen content of various SmCo samples.

Sample No.	Description	% Sm	Ball Mill Grinding Time	Wt % O_2
-	+100-mesh powder	34.5	none	0.033
-	+100-mesh powder	41.8	none	0.035
GB1	HIPed sample	35.5	15 min.	0.270
GB2	HIPed sample	36.0	15 min.	0.079
GB3	HIPed sample	35.5	2 hrs.	0.097
GB4	HIPed sample	36.0	2 hrs.	0.155

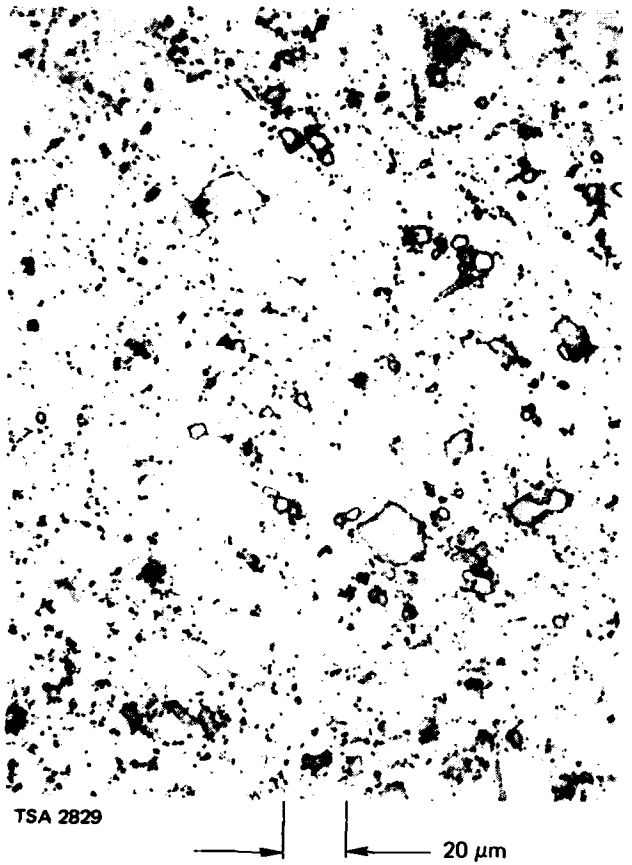

Figure 13. GB-1-35.5% Sm. Ground 15 minutes. HIPed magnet. Heat treated 1050°C-48 hours. Aged and quick cooled. 500X.

Figure 14. GB2-36.0% Sm. Ground 15 minutes. HIPed magnet. Heat treated 1050°C-48 hours. Aged and quick cooled. 500X.

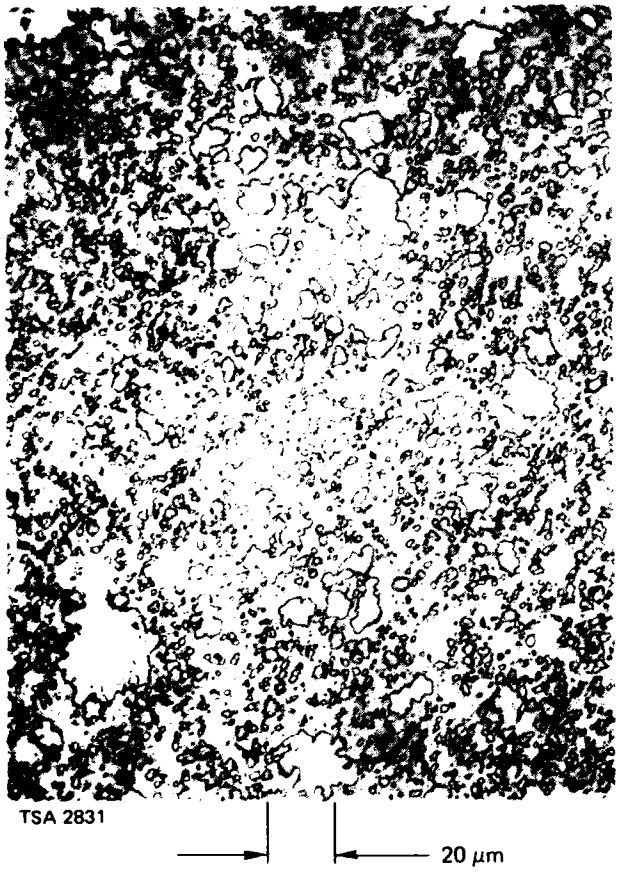

Figure 15. GB3-35.5% Sm. Ground 2 hours. HIPed magnet. Heat treated 1050°C-48 hours. Aged and quick cooled. 500X.

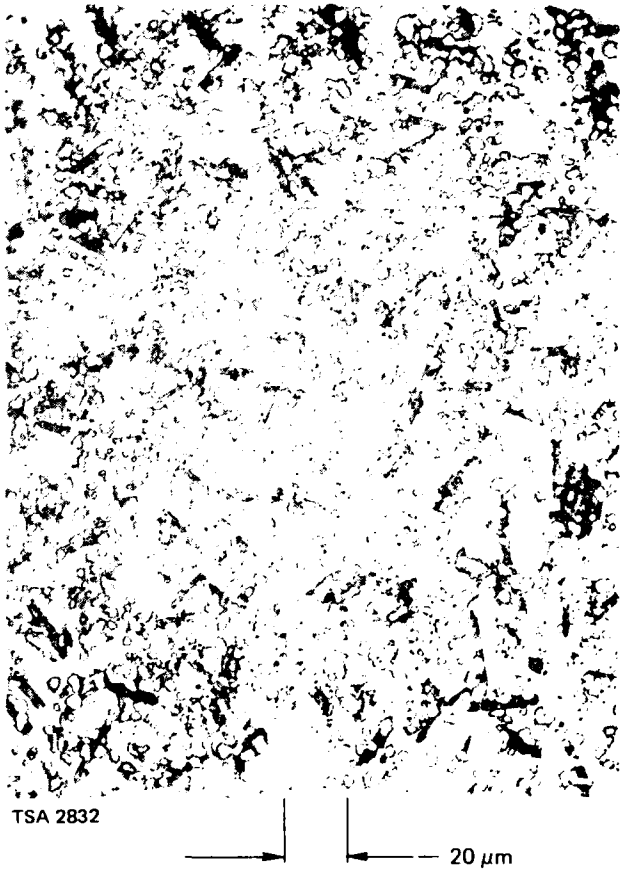

Figure 16. GB4-36.0% Sm. Ground 2 hours. HIPed magnet. Heat treated 1050°C-48 hours. Aged and quick cooled. 500X.

Table 7. Intrinsic coercivities of low oxygen $SmCo_5$ HIPed magnets.

Sample No.	Description	Heat Treatment after HIP	H_{ci}(kOe)
G.B.1	35.5% Sm, 15 min grind	As-HIPed	17.0
G.B.1	35.5% Sm, 15 min grind	1050°C-24 hrs, 900°C-120 hrs, Q.C.	55.0
G.B.1	35.5% Sm, 15 min grind	1100°C-24 hrs, 900°C-24 hrs, Q.C.	56.0
G.B.2	36.0% Sm, 15 min grind	As-HIPed	12.0
G.B.2	36.0% Sm, 15 min grind	1050°C-24 hrs, 900°C-120 hrs, Q.C.	49.5
G.B.2	36.0% Sm, 15 min grind	1100°C-24 hrs, 900°C-24 hrs, Q.C.	51.0
G.B.3	35.5% Sm, 2 hrs grind	As-HIPed	33.0
G.B.3	35.5% Sm, 2 hrs grind	1050°C-24 hrs, 900°C-120 hrs, Q.C.	22.0
G.B.3	35.5% Sm, 2 hrs grind	1100°C-24 hrs, 900°C-24 hrs, Q.C.	13.5
G.B.4	36.0% Sm, 2 hrs grind	As HIPed	33.0
G.B.4	36.0% Sm, 2 hrs grind	1050°C-24 hrs, 900°C-120 hrs, Q.C.	26.0
G.B.4	36.0% Sm, 2 hrs grind	1100°C-24 hr, 900°C-24 hrs, Q.C.	13.0

The results of the first batch of low oxygen content $SmCo_5$ magnets are quite encouraging as far as the low levels of oxygen achieved and the coercivities produced. The H_{ci} of 56 kOe measured in one of the samples is the highest ever reported for an $SmCo_5$ magnet produced by densification of $SmCo_5$ powder. An oxygen content of 0.079% in one of the magnets is almost an order of magnitude lower than what is found in commercial sintered $SmCo_5$ magnets.

The samples GB-1 and GB-2, with coarser powder, gave the higher coercivities than the samples GB-3 and GB-4 with similar compositions but finer powder. The phase compositions shown in Figures 13 through 16 show that the samples GB-1 and GB-2 have small amounts of Sm_2Co_7 and no Sm_2Co_{17}, and GB-3 and GB-4 show Sm_2Co_{17} as the second phase. Thus the microstructures account for the higher coercivities seen in GB-1 and GB-2 samples and smaller coercivities of the GB-3 and GB-4 samples.

However, the oxygen contents fail to account for the microstructures. Based on the microstructures, it appears that the sample GB-1 should have much less oxygen content and GB-3 should have higher than the measured percentages shown in Table 6. It is suspected that the oxygen analysis samples may have been mixed up. If we assume that to be the case, then it is seen that the lowering of the oxygen content has a beneficial effect on the final coercivity.

Now that we have successfully produced $SmCo_5$ magnets with very low oxygen content and also have shown that higher stability can be achieved by the elimination of the Sm_2Co_7 second phase, which can be produced by the HIP technique, it is believed that further studies should enable us to produce the desired goal of near-zero decay rates in $SmCo_5$ magnets. It is recommended that such studies should continue into the future.

SECTION 3

Sm-Co MAGNETS BY PLASMA SPRAYING

3.1 Introduction

The initial objectives of this task included an investigation of the feasibility of employing arc-plasma-spraying as a process for producing Sm_2Co_{17}-type magnets of binary Sm-Co compositions with coercivities considerably higher than the one to two kOe that are obtained through the conventional sintering process. The motivation behind this effort was the considerable success achieved with the $SmCo_5$ composition where the largest ever-to-be-measured room temperature coercivity value of 67.5 kOe was obtained.[7] The energy product of the sprayed $SmCo_5$ magnets, however, was limited to values of about 9 MGOe, mainly because these magnets were close-to-isotropic in structure. To obtain a higher level of flux from the sprayed magnets, one therefore needed to either introduce texture in the deposits or shift the material composition toward higher cobalt content (by the spraying of Sm_2Co_{17}-type deposits).

The approach that was taken initially (as stated above) was to attempt to produce Sm_2Co_{17}-type magnets with reasonably high coercivities. It was hoped that this would permit the fabrication of close-to-isotropic sprayed magnets with energy products of roughly 12 MGOe in a manner similar to the 9 MGOe value that was achieved with the $SmCo_5$ composition. Experiments performed toward this end showed that even though somewhat higher coercivities (higher than what are observed in sintered materials) were achievable in the sprayed samples, the improvements were not significant to the extent that the second quadrant characteristics remained poor.[3] The highest value for the maximum energy product that was measured in these sprayed Sm_2Co_{17}-type compositions was 6.6 MGOe. Therefore, it appeared that to attain energy products well in excess of the 7 to 9 MGOe that have been achieved in

$SmCo_5$ compositions, it was important to produce crystallographically aligned deposits (of the $SmCo_5$ or the Sm_2Co_{17}-type stoichiometries) with the unique c-axis, which is also the easy axis of magnetization, preferably oriented in a direction perpendicular to the plane of deposition. Substantial efforts have therefore been expended at attempting to produce such aligned deposits using a variety of techniques with some preliminary encouraging results. These efforts were expanded to include additional compositions in the range defined by the stoichiometries of the $SmCo_5$ and Sm_2Co_{17} compounds because of their combined potential to produce high quality sprayed magnets. Results obtained toward this end over the past year are included in this report.

The Plasma Spray Process

A schematic sketch of this process is shown in Figure 17.

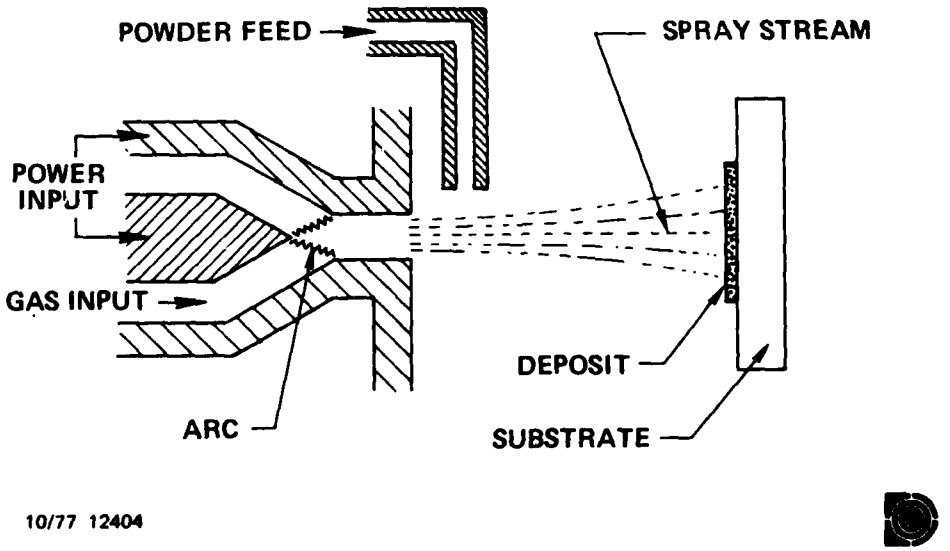

Figure 17. Schematic sketch of the plasma spray process.[8]

The process involves striking a high intensity dc arc between two electrodes, and ionization of gases - nitrogen, hydrogen, argon, and helium - as a consequence. This forms the plasma. Upon exit through a nozzle, the plasma combines to form neutral atoms, and releases a large amount of thermal energy without an appreciable loss in gas temperature. The material to be deposited is introduced at this stage in the form of a powder. The gases impart both thermal and kinetic energy to the powder particles, thereby melting them and propelling them rapidly towards the substrate to form the deposit.

3.2 Objective

The current goal of this effort, as stated earlier, is to produce aligned plasma-sprayed deposits of the $SmCo_5$ and Sm_2Co_{17}-type stoichiometries with the aim of being able to fabricate sprayed Sm-Co magnets with energy products well in excess of 9 MGOe.

3.3 Previous Work

Five starting powder compositions, in the range of 26.0 to 34.0 weight percent samarium, were selected and sprayed on water cooled copper substrates inside an inert gas environment plasma spray chamber. It was expected that the compositions of the deposited materials would be close to Sm_2Co_{17} with deposit compositions on either side of stoichiometry. X-ray diffraction patterns were obtained on a few of the deposits with copper radiation and a diffracted beam graphite monochromator. Considerable broadening of the X-ray peaks was observed for all of the deposits. The diffuse patterns obtained on these materials were believed to be indicative of amorphous structures similar to what are conventionally obtained by rapid quenching techniques.

Several low temperature treatments were employed for optimizing the magnetic properites of the deposited materials. The maximum value of coercivity was measured as 7.9 kOe on a sample produced using the

starting powder composition of 34.0 weight percent samarium. The other magnetic properties measured for this sample were B_R = 6500 G, H_c = 4050 Oe, and $(BH)_{Max}$ = 6.6 MGOe. These studies showed that grain size played a strong role in determining the value of H_{ci} in these binary Sm_2Co_{17}-type compositions. The improvements in the magnetic properties from the low temperature treatments were attributed to increased homogenization and grain growth through crystallization related processes.

A few minor crystalline X-ray peaks were observed superimposed on an otherwise amorphous pattern in several of the deposits. In one sample, however, a single, sharp, crystalline peak was found superimposed on an otherwise amorphous-type pattern. A single peak was interpreted as illustrative of texture in the crystalline component of the deposit. The composition of the deposit, as measured by the X-ray fluorescence technique, was indicated to be about 30.0 weight percent samarium (which is in the two-phase $SmCo_5$ - Sm_2Co_{17} region of the phase diagram). The sole crystalline peak observed was found to be located at the (00.6) peak position for Sm_2Co_{17} - the compound of interest. This observation showed that if proper cooling conditions were maintained at the substrate it might be possible to produce crystallographically aligned Sm_2Co_{17} materials by plasma spraying. Additional deposits formed with the aim of duplicating this observation met with little success.

Most of the deposits formed subsequent to the above efforts appeared to be more crystalline than the previous deposits. Additional cooling of the the substrate through the use of liquid-nitrogen-chilled helium gas also did not appreciably alter this situation. The X-ray peaks were still very broad, indicating that the grain size was extremely small. These deposits were fabricated with starting powder compositions of 42.0, 34.5, and 28.3 weight percent samarium resulting in deposit compositions corresponding closely to the $SmCo_5$, two-phase $SmCo_5$ + Sm_2Co_{17}, and Sm_2Co_{17} stoichiometries. Samples from all of these deposits were subjected to a low temperature exposure to hydrogen gas.

It was determined that the hydriding process resulted in a removal of the low level of crystallinity that existed in the as-sprayed condition. It was therefore decided to use the hydrogen-treated as well as the as-sprayed material for studies relating to inducing crystal orientation in the deposit.

Some initial experiments toward achieving alignment were performed with as-sprayed and hydrogen-treated samples by subjecting them to a large (80 kOe) dc magnetic field at MIT's Francis Bitter National Magnet Laboratory during the process of crystallization and grain growth which occurs at temperatures of about 500°C in these compositions. These experiments indicated that whereas some improvement had probably occurred in the sample produced from the 42.0 weight percent samarium alloy powder, the other two samples suffered deterioration in properties. It was concluded that additional experiments needed to be performed before firm conclusions could be reached with respect to the effect of applied magnetic fields on influencing alignment in the crystallized deposit.

3.4 Present Work

Most of the work performed this past year was devoted to efforts aimed at producing crystallographically oriented Sm-Co deposits. A substantial amount of effort was spent on crystallizing as-sprayed and hydrogen-treated deposits produced from starting powder compositions of 42.0, 34.5 and 28.3 weight percent samarium while under the influence of externally applied dc magnetic fields and temperature gradients. Some initial experimentation was also performed, which included deposition of the 42.0 weight percent samarium alloy powder, at elevated substrate temperatures. Also included in this year's effort was transmission electron microscopy (TEM) examination of the sprayed sample that had shown a single, sharp crystalline X-ray peak located at the (00.6) peak position of the Sm_2Co_{17} compound. This sample had been reported upon earlier.[3]

3.4.1 TEM Examination of As-Sprayed Sample 253

As stated above, the X-ray pattern obtained from this sample had shown the existence of a single (00.6) peak of Sm_2Co_{17}. Therefore, it was suspected that this was associated with the presence of a very small amount of aligned crystalline Sm_2Co_{17} material possibly dispersed as crystallites in an otherwise amorphous matrix. To gain further insight into the microstructure of this deposit it was decided to examine it using the TEM technique.

The samples were analyzed using a JEOL 200 CX TEM unit operating at 200 keV. Sample preparation included mechanical thinning of 3-mm discs removed from the sprayed material using electrical discharge machining (EDM). The mechanical thinning operation was conventionally done on coarse SiC papers followed by additional lapping using diamond-containing compounds. The final thinning operation, however, was performed using an ion milling apparatus with argon ions bombarding the surface under an applied voltage of 6 keV. Suitable foils were thus obtained for TEM examination.

Figures 18 and 19 are typical of the fine granular structure that was observed in parts of the deposit. These micrographs consisted primarily of coarse (1 to 10μm) unmelted particles [that are known to exist in the microstructure from optical microscopy[7]] surrounded by very fine grains of roughly 50Å size. Diffraction patterns obtained from a fine-grained (50Å) area and from a large-grained (1 to 10μm) area, respectively, are shown in Figures 20 and 21. The fine-grained region showed a polycrystalline diffraction pattern with peak positions indicative of the $SmCo_5$ structure. The single crystal pattern observed (superimposed over an extremely broad diffraction pattern) was consistent with the Sm_2Co_{17} structure, with the pattern being (110) in hcp.

Figure 18. TEM micrograph of region A in sample 253.

CD 29570

500Å

Figure 10. TEM micrograph of region B in sample 253.

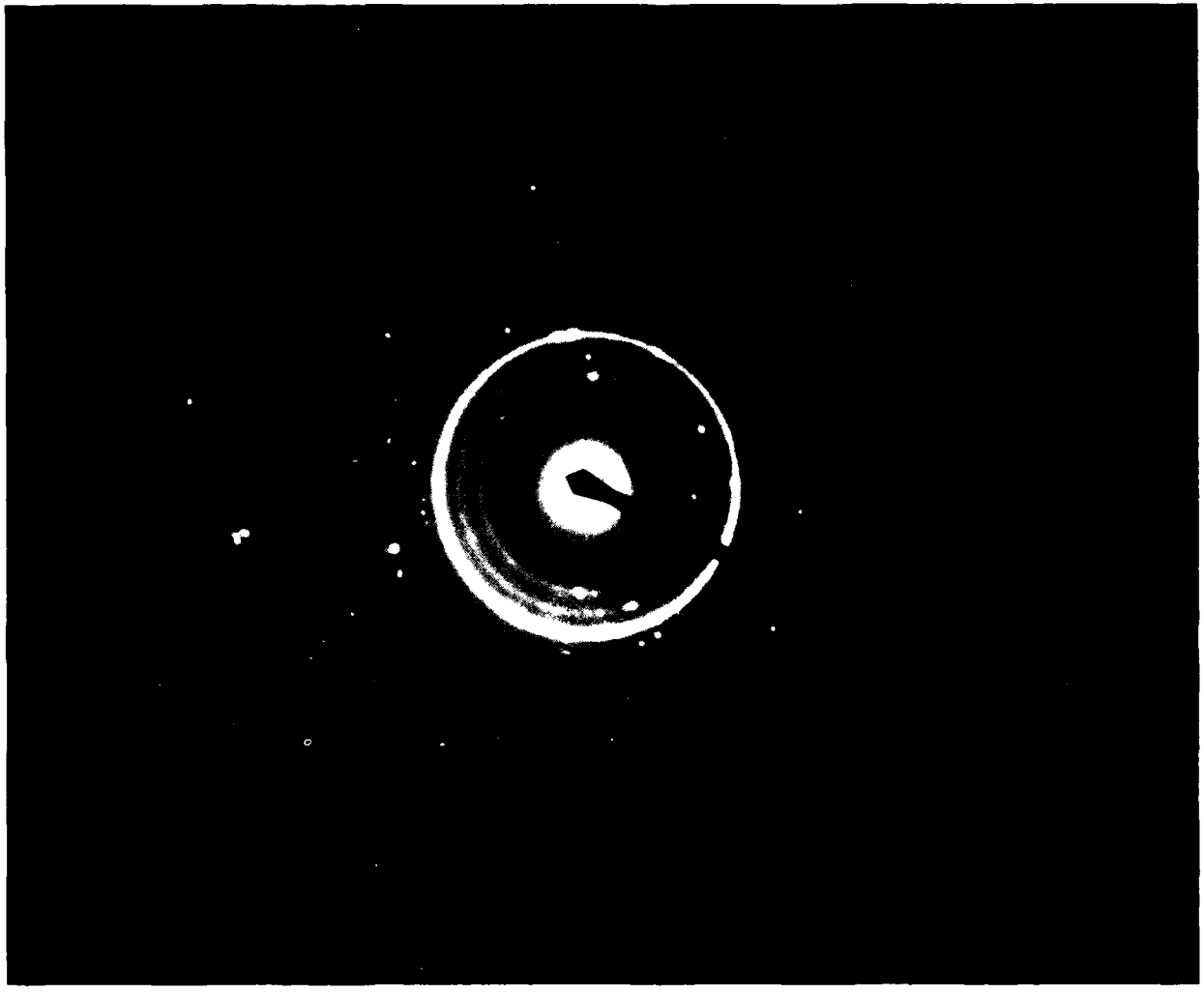

CD29571 Figure 20. Diffraction pattern obtained from fine-grained region.

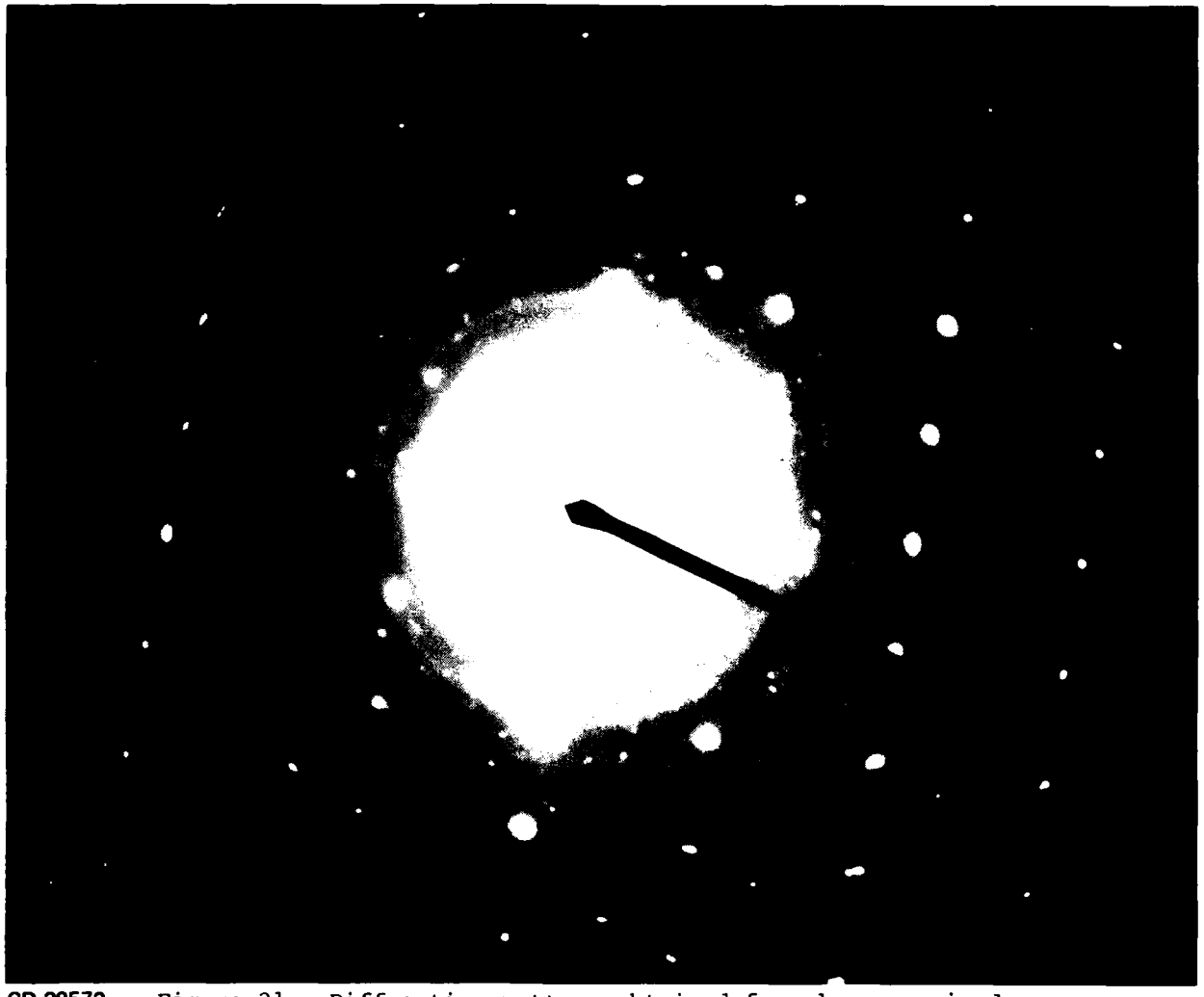

CD 29573 Figure 21. Diffraction pattern obtained from large-grained area.

Amorphous regions were also observed in the as-deposited material as indicated by the extremely diffuse pattern obtained from one such region shown in Figure 22. No attempt was made to quantify the relative fractions of the differently occurring microstructures. It was concluded that a substantial level of effort, which would include statistical sampling of the material, would be required to identify specific aligned crystallites that contributed to the (00.6) peak on the X-ray diffraction pattern.

3.4.2 Alignment Studies

A reasonably extensive level of effort was expended in efforts aimed at producing sprayed deposits which possess crystallographic alignment and, therefore, display anisotropic magnetic behavior. Procedures examined for influencing texture in the deposit included thermal treatment of amorphous and near-amorphous deposits while under the influence of externally applied dc magnetic fields and temperature gradients, and deposition on substrates maintained at elevated temperatures. All of the work performed with respect to magnetic and temperature gradient annealing during this reporting period was performed on 500°C hydrogen-treated materials because removal of a low level of existing crystallinity in the as-sprayed condition is known to occur by following such a procedure that renders the deposit substantially more amorphous.[4] It was believed that a more amorphous deposit would be more conducive to responding favorably to attempts aimed at producing aligned material.

Plasma spray deposits made from powders of the following Sm-Co alloy compositions were used in the studies on magnetic and temperature gradient annealing: (1) 42.0 wt % Sm, (2) 34.5 wt % Sm, and (3) 28.3 wt % Sm. The stoichiometric intermetallic compounds $SmCo_5$ and Sm_2Co_{17} contain 33.9 wt % and 23.1 wt % Sm, respectively. Because of evaporation and oxygen-related samarium losses during plasma spraying, compositions (1) and (3) normally produce deposits of close to stoichiometric $SmCo_5$ and Sm_2Co_{17} respectively, and the intermediate composition (34.5 wt % Sm) powder produces a deposit which is in the two-phase ($SmCo_5$ + Sm_2Co_{17}) region. The selection of the above compositions therefore gave a comprehensive range for the study.

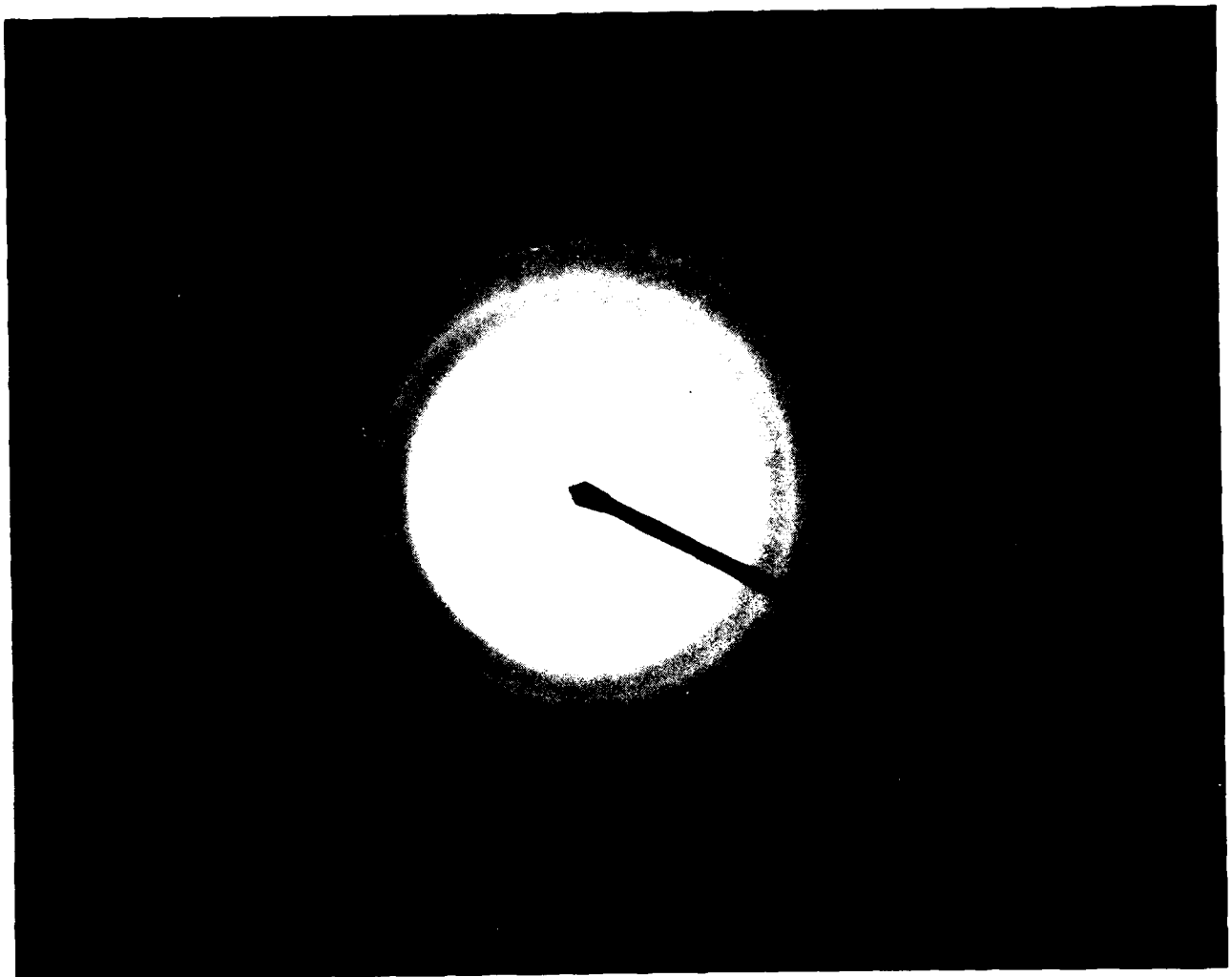

CD 29569 Figure 22. Amorphous-type pattern obtained from sample 253.

3.4.2.1 Thermal Treatment in a Magnetic Field

As discussed in last year's report,[4] the present effort deals with the crystallization of plasma sprayed Sm-Co alloy deposits in an applied high strength magnetic field. The crystallization temperature for amorphous deposits is close to 500°C. Therefore, if an amorphous plasma spray deposit is heated from room temperature to an elevated temperature past 500°C in a strong dc magnetic field, the crystal nuclei formed might have their c-axes parallel to the applied field. As these nuclei grow by incorporating the surrounding amorphous alloy into their crystal lattices, a preferred orientation in the mass can result with the c-axis of the various grains oriented parallel to each other (and in the direction of the applied magnetic field) and random orientation of the basal planes perpendicular to the c-axis.

A six-inch-bore Bitter magnet capable of producing a dc magnetic field strength of about 80 kOe was made available by the National Magnet Laboratory of MIT for this study. An available furnace capable of operating inside the Bitter magnet was modified for carrying out magnetic annealing experiments. A schematic sketch of this furnace was shown in Reference 4. The cylindrical furnace fitted snugly in the bore of the six-inch magnet. The sample was located inside a stainless steel tube at the peak position of the magnetic field and was heated by four SiC rods. Temperature control and rate of rise of temperature were controlled manually using a Variac power supply. The temperature of the sample was determined by a thermocouple located inside the furnace tube adjacent to the magnet sample. The outer shell of the furnace was water-cooled to prevent undue heating of the Bitter magnet.

Static, dc magnetic fields of 65 to 80 kOe field strength were applied to the samples prior to the rise in temperature. The temperature was raised by manual control of a Variac which supplied power to the furnace. Many problems were encountered during these experiments, mainly relating to electrical opens that resulted in the circuit. This limited the maximum temperature achieved to low

undesirable values, beyond which the runs had to be discontinued. The typical rate of rise in temperature achieved during these experiments and problems related to achieving acceptable furnace operation are shown in Figure 23. Figure 24 shows one good run that was attained during this experimentation. In each of these, and other, many runs, the same set of samples was used over and over again, with the samples oriented in identical fashion with respect to the applied magnetic field, because the effect of each individual run was expected to only add to any induced crystallographic texture that may have developed earlier and not interfere with it in any manner.

The different samples were measured for their magnetic properties following the magnetic annealing run shown in Figure 24. The results of these measurements are shown in Table 8. These results showed that this procedure failed to induce the desired alignment of the crystal axis in the several crystallites. It is suspected that the increased coercivity that was observed earlier, from a similar magnetic annealing run which was performed to a maximum indicated temperature substantially lower than the 910°C achieved in this effort, must have resulted from exposure to a temperature higher than was indicated by the thermocouple reading. (The lack of alignment in the magnetically annealed deposits was inferred both from the low B_R values that were measured as well as the shape of the $4\pi M$ versus H curves in the first quadrant.)

3.4.2.2 Annealing in a Temperature Gradient

Several 0.2-inch-diameter and about 0.125-inch-long disc-shaped samples, similar to those used for the magnetic annealing studies, were removed from the hydrogen-treated deposits made with 42.0, 34.5, and 28.3 weight percent samarium starting powder compositions. These were then used for annealing experiments performed while a temperature gradient was applied simultaneously to the specimen.

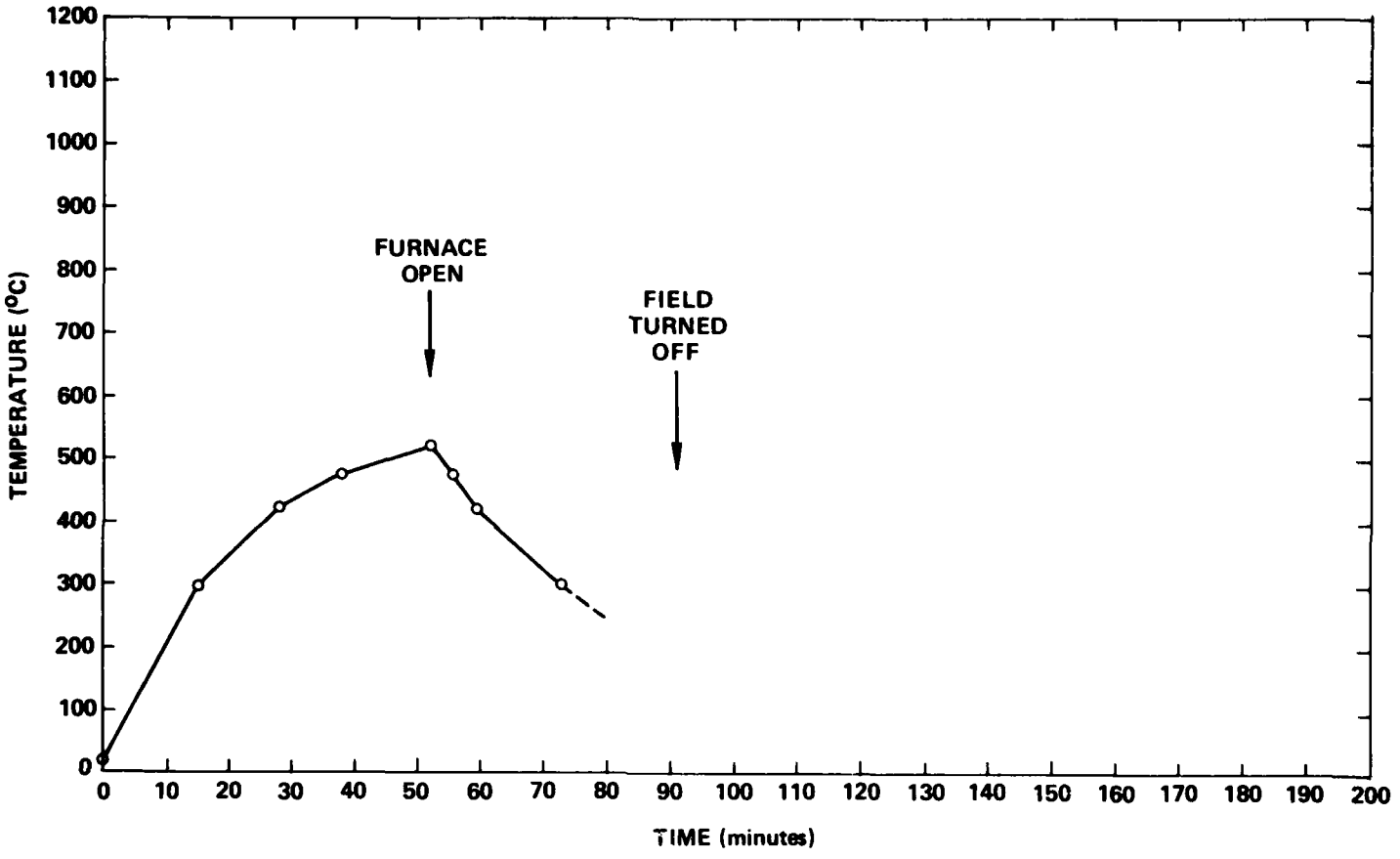

12/82 CD29551

Figure 23. Typical rate of rise in temperature and low temperature achieved in initial runs. Applied field strength was 80 kOe.

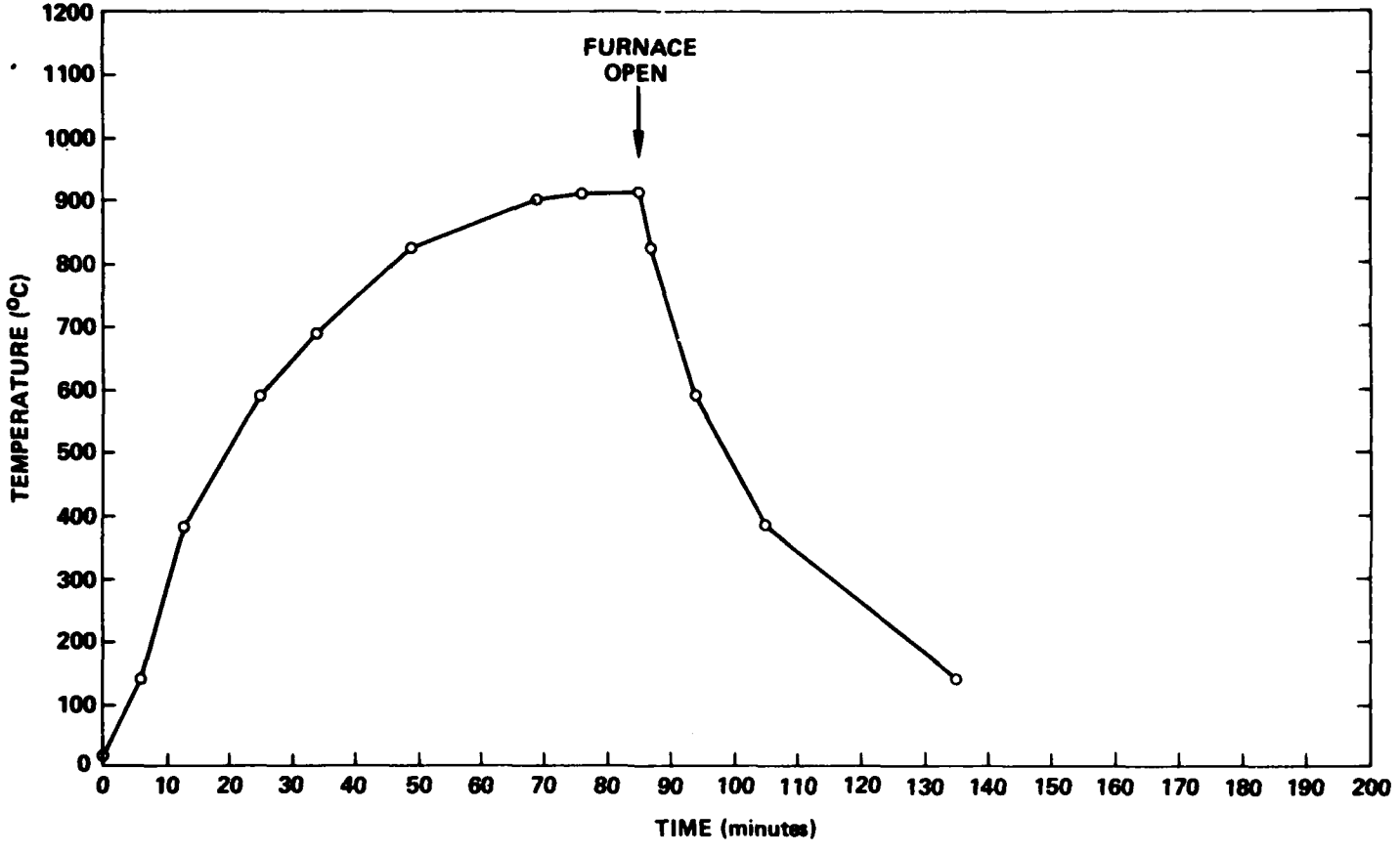

12/82 CD29553

Figure 24. Improved conditions obtained with respect to attainment of higher maximum temperature. Applied magnetic field was 68.3 kOe.

Table 8. Magnetic properties of magnetically annealed samples.

Sample No.	% Sm in Powder	Heat Treatment Condition	B_R(G)	H_{ci}(kOe)	Remarks (4πM versus H Curves)
266.1.2	42.0	Multiple magnetic annealing runs. Maximum temperature ~ 910°C.	4000	47.5	No indication of alignment
275.1.2	34.5	Multiple magnetic annealing runs. Maximum temperature ~ 910°C.	5154	4.5	No indication of alignment
277.1.2	28.3	Multiple magnetic annealing runs. Maximum temperature ~ 910°C.	5330	2.2	No indication of alignment

The experiments were performed inside a clean, bakeable, stainless steel chamber. The chamber was evacuated to the level of about 1μm range vacuum using a mechanical and diffusion pump system and back-filled with argon gas to a pressure roughly one $lb/in.^2$ above atmospheric. A net positive pressure was assured by constant outflow of argon gas from the chamber which was measured and maintained at about one liter per minute using a flow meter.

A photograph of the apparatus (which is normally enclosed within the stainless steel chamber during runs) in which the temperature gradient runs were accomplished is shown in Figure 25. One flat surface of the disc sample was maintained in intimate contact with a water-chilled copper block while the other surface contacted a steel block that was heated by induction using an energized rf coil surrounding the steel block. Initially, the sample was held between the copper and steel blocks using a set of four screws threaded into the steel block (after passing through appropriate holes in the copper block). This was subsequently modified to include spring loading of the cold copper block to ensure that the assembly always remained such that the respective faces were always in intimate contact with each other irrespective of the thermal expansion characteristics of the several parts. The temperatures of the copper block and the stainless steel block were measured both using chromel-alumel thermocouples attached to these respective parts. In some instances an open junction was indicated for the thermocouple attached to the stainless block.

Very little interference was observed in the thermocouple data from effects related to the presence of an rf field. This was confirmed by the use of an optical pyrometer for measuring the high temperatures of the stainless steel block. The measurements were made by focussing the optical pyrometer onto the image of the glowing red-hot stainless steel block in a mirror placed behind the rear viewing window of the stainless steel chamber. Typical rate of rise in temperature as measured using the optical pyrometer and thermocouple on the hot block and a thermocouple on the cold block is shown in Figure 26. It should be noted that the optical pyormeter data correlated well with the thermocouple results.

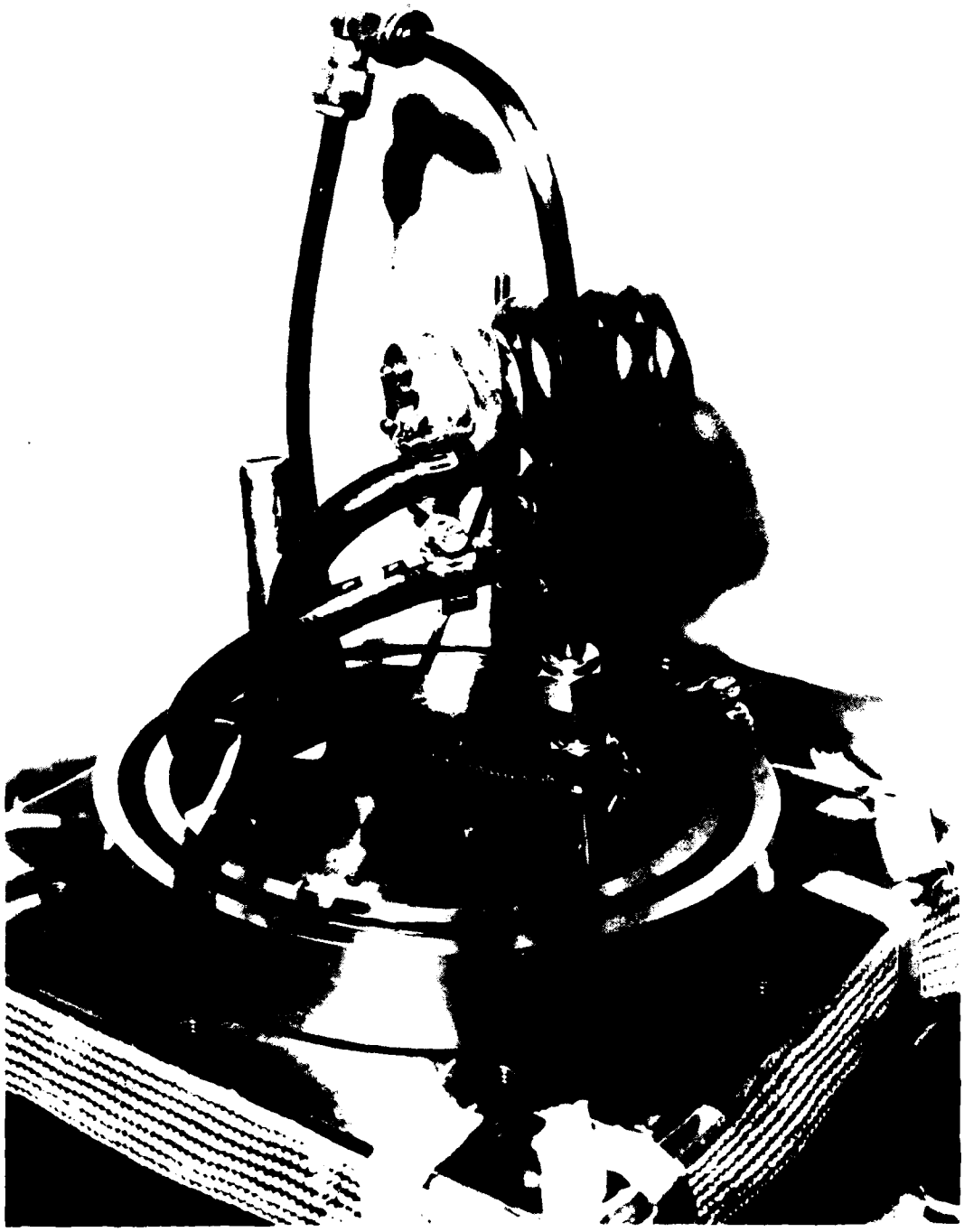

12/82 CD29647

Figure 15. Temperature gradient annealing apparatus.

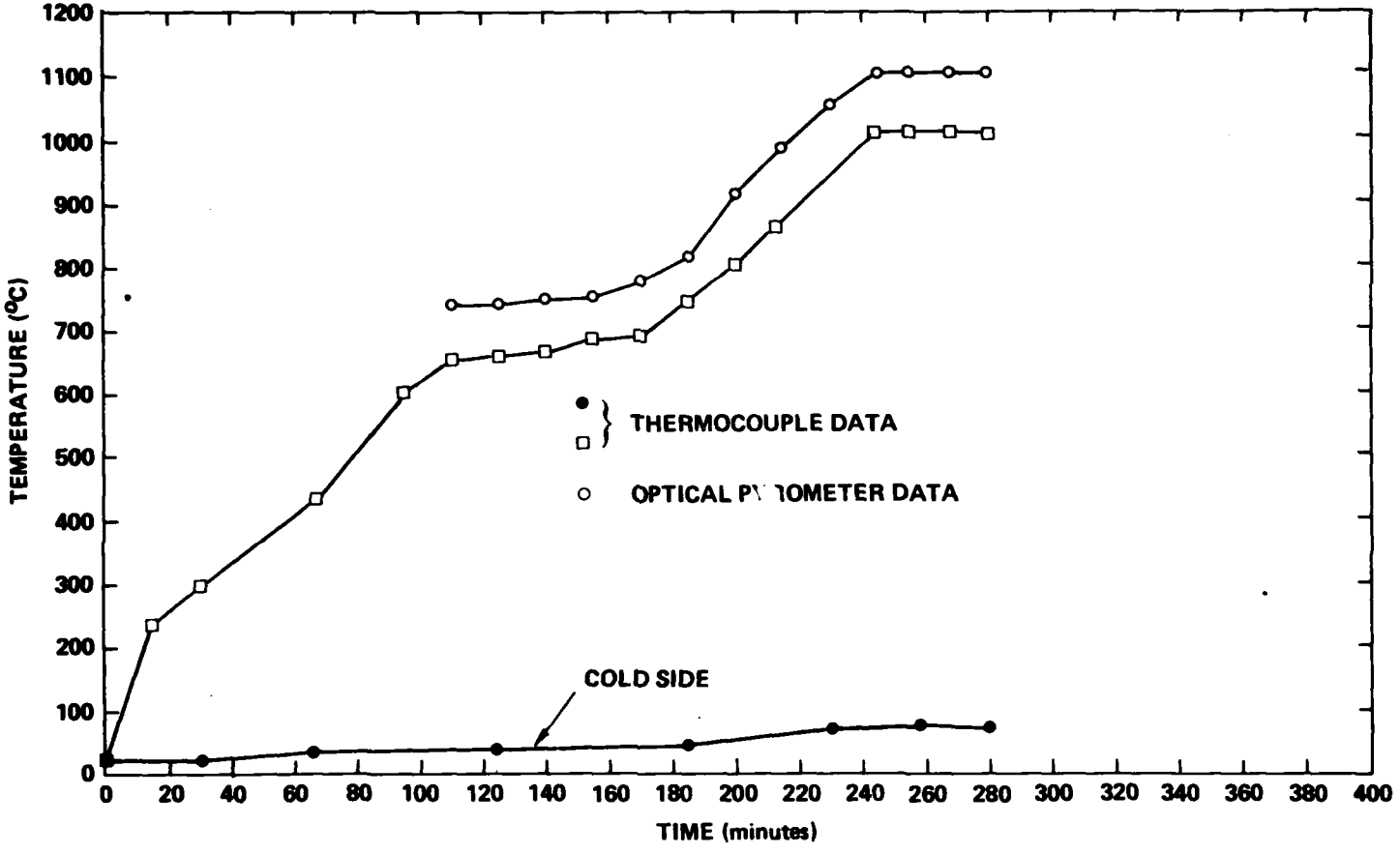

Figure 26. Typical temperature gradient annealing run.

A constant overestimate of the temperature (of about 75 to 100°C), as provided by the optical pyrometer, was attributed to unknown variables, such as the emissivity of the stainless block. It should also be noted that the samples were continuously annealed, during the experiments, under the effect of an increasing temperature gradient with rise in temperature of the hot side. (This was facilitated by the success achieved in maintaining a low temperature value for the cold copper block.)

X-ray diffraction patterns were obtained on these deposits following the temperature gradient annealing experiments. These patterns, like those reported earlier, were obtained using copper radiation with a graphite monochromator located on the diffracted beam. This minimizes effects related to processes such as fluorescence of the sample by the incident radiation. Patterns typical of what was observed are shown for two samples in Figure 27. The peaks in general were not resolved properly, even though some samples appeared to indicate preferential peak development on the hot side, and the data were considered ambiguous at best. Magnetic measurements failed to resolve this discrepancy (see Table 9). The low B_R values noted in Table 9 would suggest isotropic behavior; however, a quick saturation of some of these deposits at relatively low applied fields (low compared to the anisotropy field of these materials), in the first quadrant of the $4\pi M$ versus H loops, leaves that issue somewhat ambiguous. It is possible that the bulk of the magnet was still substantially near-amorphous (even after the gradient runs that were performed). The X-ray patterns in Figure 27 would tend to support this in that the patterns were obtained at a distance of roughly 0.001 inch away from the original surface. This minimized effects related to a metallurgical reaction between the intimately contacting parts as well as effects arising from any low level of impurity present in the argon gas.

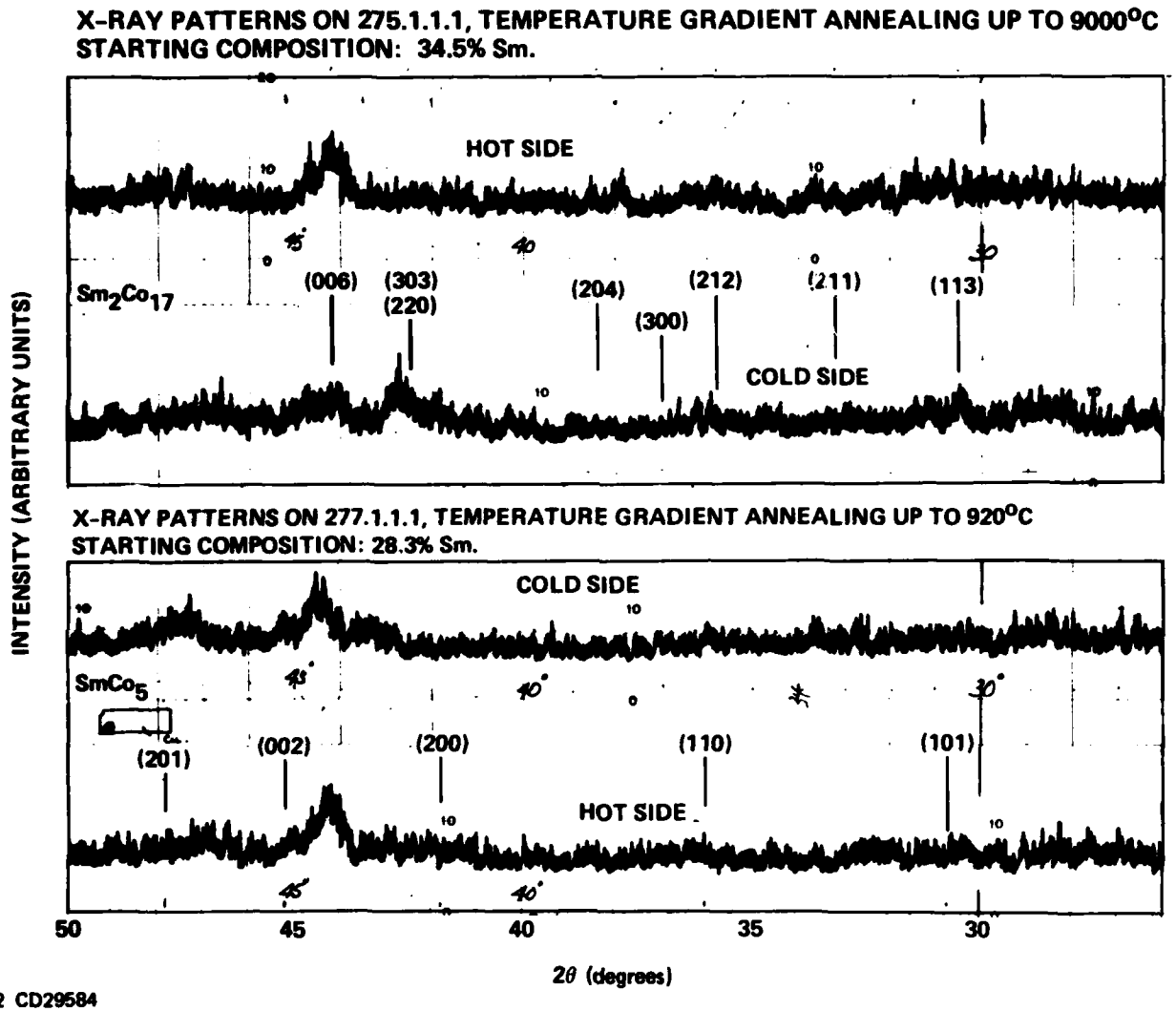

Figure 27. X-ray diffraction patterns obtained on two samples as indicated. Cu radiation.

Table 9. Magnetic properties of temperature gradient samples.

Sample No.	% Sm in Powder	Heat Treatment in Condition*	B_R(G)	H_{ci}(kOe)
277.1.1.2	42.0	Temperature gradient up to 760° + 1140°C (30 April 1982)	4950	45.0
266.1.3.1	42.0	Temperature gradient to 1130°C	6100	2.25
266.1.3.2	42.0	266.1.3.1 + reverse temperature gradient to 1100°C	4600	3.0
275.1.1.1	34.5	Temperature gradient to 908°C	5230	2.5
275.1.1.2	34.5	275.1.1.1 + reverse temperature gradient to 1100°C	3120	2.5
277.1.1.2	28.3	Temperature gradient to ~ 950°C + 1140°C		~0
277.1.3.1	28.3	Temperature gradient to 1120°C	6650	1.1
277.1.3.2	28.3	277.1.3.1 + reverse temperature gradient to 1100°C		~0

* Temperatures as indicated by the optical pyrometer

3.4.2.3 Depositions at High Substrate Temperatures

Some initial investigations were performed on steel substrates maintained at elevated temperatures using a starting powder composition of 42.0 weight percent samarium. The high substrate temperatures were obtained by heating up the substrate with the incident plasma flame (while no alloy depositons were being performed). The substrates consisted of steel samples of different length which were mounted onto a water-cooled feedthrough located inside the plasma-spray chamber. Heat conduction from the surface was therefore directly influenced by the length of the substrate (over which heat was conducted) and this resulted in the achievement of a variety of substrate temperatures. The temperature of the substrate was determined with a thermocouple attached to it while it was stationary and exposed to the plasma flame. Once the equilibrium temperature was measured, the thermocouple was disconnected and the substrate allowed to rotate, then heated again for the predetermined period of time needed to allow equilibration of the temperature, and the depositions were performed by introducing the alloy powder into the plasma flame.

The deposited materials were examined for alignment using X-ray diffraction with copper radiation and a diffracted beam graphite monochromator. The results obtained were quite dramatic and are shown in Figure 28. It was observed that c-axis alignment of the $SmCo_5$ deposit was indeed achieved using this procedure with greater crystallographic alignment [as indicated by the strong (002) peak of $SmCo_5$] occurring with increasing temperatures. It is suspected that an optimum substrate temperature condition exists for a given alloy powder with a given composition and size distribution. These will be needed to be optimized for producing good quality sprayed $SmCo_5$ magnets.

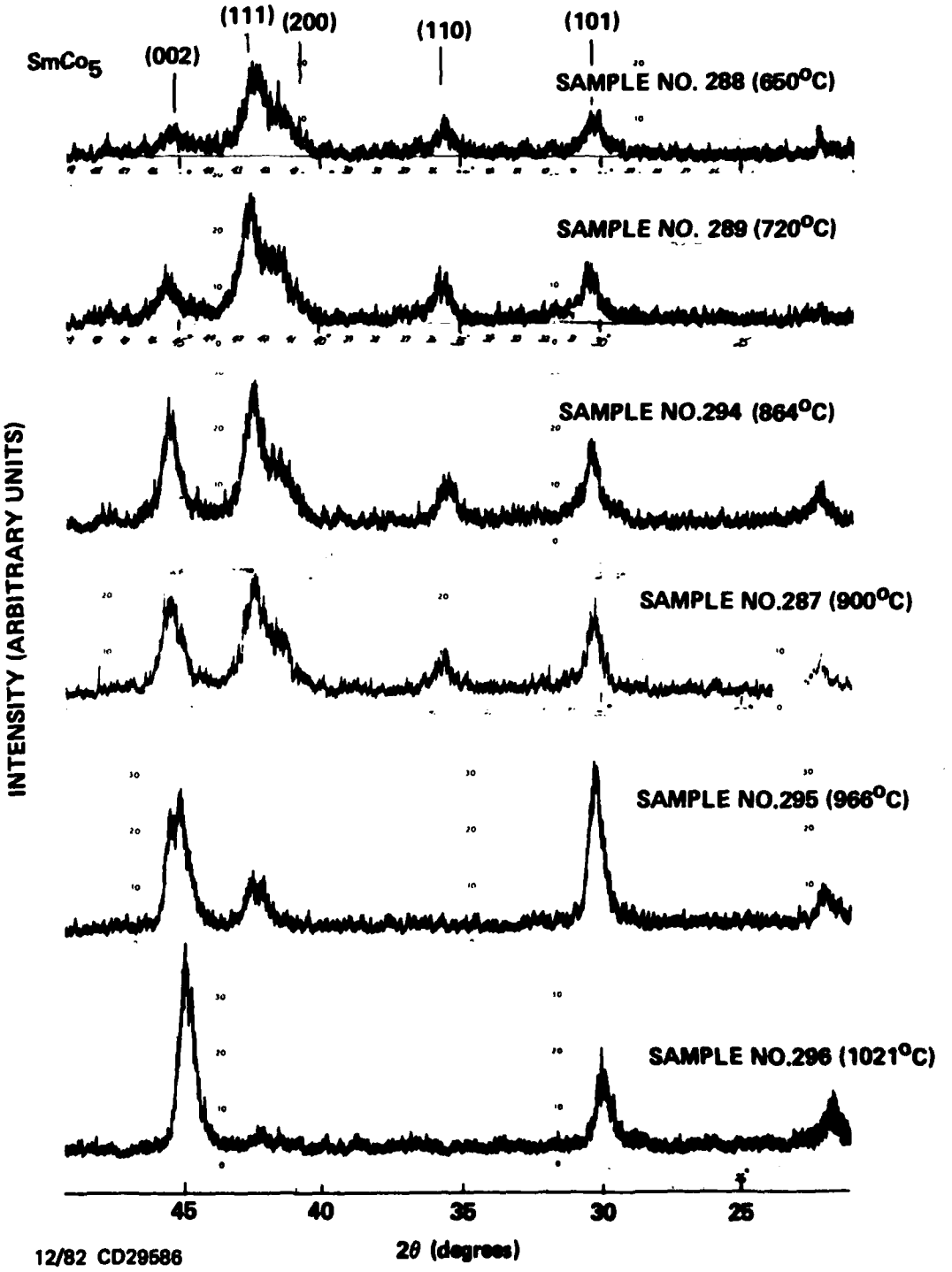

Figure 28. Effect of substrate temperature on alignment in sprayed SmCo deposits. Cu radiation.

The achievement of the c-axis orientation in $SmCo_5$ in a direction perpendicular to the plane of deposition (which is parallel to the spray direction) is considered a major breakthrough in the fabrication process development of these magnets. Because the spray process is a lower cost procedure for producing magnets in complex geometries and shapes (due to its near-net shape and size capability), it is expected that good quality magnets produced using this procedure will find extensive applications in the production of such magnets for a variety of applications. Further effort under this program will therefore concentrate on optimizing the spray process and thermal treatment variables to produce the high quality magnets that now appear possible by this lower cost procedure.

LIST OF REFERENCES

1. Das, D., E. Wettstein, and K. Kumar, Materials Research for Advanced Inertial Instrumentation, Task 3: Rare Earth Magnetic Material Technology as Related to Gyro Torquers and Motors (Technical Report No. 1), Charles Stark Draper Laboratory Report R-1177, July 1978. Office of Naval Research Contract N00014-77-C-0388.

2. Das, D., K. Kumar, and E. Wettstein, Materials Research for Advanced Inertial Instrumentation, Task 3: Rare Earth Magnetic Material Technology as Related to Gyro Torquers and Motors (Technical Report No. 2), Charles Stark Draper Laboratory Report R-1306, October 1979. Office of Naval Research Contract N00014-77-C-0388.

3. Das, D., K. Kumar, and E. Wettstein, Materials Research for Advanced Inertial Instrumentation, Task 3: Rare Earth Magnetic Material Technology as Related to Gyro Torquers and Motors (Technical Report No. 3), Charles Stark Draper Laboratory Report R-1435, December 1980. Office of Naval Research Contract N00014-77-C-0388.

4. Das, D., K. Kumar, E. Wettstein, Materials Research for Advanced Inertial Instrumentation, Task 3: Rare Earth Magnetic Material Technology as Related to Gyro Torquers and Motors (Technical Report No. 4), Charles Stark Draper Laboratory Report R-1529, December 1981. Office of Naval Research Contract N00014-77-C-0388.

5. Benz, M.G., R.P. Laforce, and D.L. Martin, AIP Conf. Proc. No. 18, 1974, p. 1173.

6. Mildrum, H.F., and D.J. Idell, Goldschmidt Informiert, 4/75, No. 35, December 1975, p. 54.

7. Kumar, K., D. Das, and E. Wettstein, J. Appl. Phys., 49 (3), 1978, p. 2052.

8. Kumar, K., and D. Das, Thin Solid Films, 54 (3), 1978, p. 263.

BASIC DISTRIBUTION LIST

Organization	Copies
Defense Documentation Center Cameron Station Alexandria, VA 22314	12
Office of Naval Research Department of the Navy 800 N. Quincy Street Arlington, VA 22217	
ATTN: Code 471	1
Code 102	1
Code 470	1
Commanding Officer Office of Naval Research Branch Office Building 114, Section D 666 Summer Street Boston, MA 02210	1
Commanding Officer Office of Naval Research Branch Office 536 South Clark Street Chicago, IL 60605	1
Naval Research Laboratory Washington DC 20375	
Attn: Codes 6000	1
6100	1
6300	1
6400	1
2627	
Naval Air Development Center Code 302 Warminster, PA 18964 ATTN: Mr. F.S. Williams	1
Naval Postgraduate School Monterey, CA 93840 ATTN: Mechanical Engineering Department	1

Organization	Copies
Naval Air Propulsion Test Center Trenton, NJ 08628 ATTN: Library	1
Naval Construction Batallion Civil Engineering Laboratory Port Hueneme, CA 93043 ATTN: Materials Division	1
Naval Electronics Laboratory San Diego, CA 92152 ATTN: Electron Materials Science Division	1
Naval Missile Center Materials Consultant Code 3312-1 Point Mugu, CA 92041	1
Commanding Officer Naval Surface Weapons Center White Oak Laboratory Silver Spring, MD 20910 ATTN: Library	1
David W. Taylor Naval Ship Research and Development center Materials Department Annapolis, MD 21402	1
Naval Undersea Center San Diego, CA 92132 ATTN: Library	1
Naval Underwater System Center Newport, RI 02840 ATTN: Library	1
Naval Weapons Center China Lake, CA 93555 ATTN: Library	1

BASIC DISTRIBUTION LIST (Continued)

Organization	Copies
Naval Air Systems Command Washington, DC 20360 ATTN: Codes 52031 52032	1
Naval Sea System Command Washington, DC 20362 ATTN: Code 035	1
Naval Facilities Engineering Command Alexandria, VA 22331 ATTN: Code 03	1
Scientific Advisor Commandant of the Marine Corps Washington, DC 20380 ATTN: Code AX	1
Naval Ship Engineering Center Department of the Navy Washington, DC 20360 ATTN: Code 6101	1
Army Research Office P.O. Box 12211 Triangle Part, NC 27709 ATTN: Metallurgy and Ceramics Program	1
Army Materials and Mechanics Research Center Watertown, MA 02172 ATTN: Research Programs Office	1
Air Force Office of Scientific Research Bldg. 410 Bolling Air Force Base Washington, DC 20332 ATTN: Chemical Science Directorate	1
Electronics & Solid State Sciences Directorate	1
Air Force Materials Laboratory Wright-Patterson AFB Dayton, OH 45433	1

Organization	Copies
NASA Headquarters Washington, DC 20546 ATTN: Code RRM	1
NASA (216) 433-4000 Lewis Research Center 21000 Brookpark Road Cleveland, OH 44135 ATTN: Library	1
National Bureau of Standards Washington, DC 20234 ATTN: Metallurgy Division	1
Inorganic Materials Division	1
Director Applied Physics Laboratory University of Washington 1013 Northeast Fortieth Street Seattle, WA 98105	1
Defense Metals and Ceramics Information Center Battelle Memorial Institute 505 King Avenue Columbus, OH 43201	1
Metals and Ceramics Division Oak Ridge National Laboratory P.O. Box X Oak Ridge, TN 37380	1
Los Alamos Scientific Laboratory P.O. Box 1663 Los Alamos, NM 87544 ATTN: Report Librarian	1
Argonne National Laboratory Metallurgy Division P.O. Box 229 Lemont, IL 60439	1
Brookhaven National Laboratory Technical Information Division Upton, Long Island New York 11973 ATTN: Research Library	1

BASIC DISTRIBUTION LIST (Continued)

Organization	Copies	Organization	Copies
Library Building 50, Room 134 Lawrence Radiation Laboratory Berkeley, CA	1	Office of Naval Research Branch Office 1030 East Green Street Pasadena, CA 91106	1

SUPPLEMENTARY DISTRIBUTION LIST

Technical and Summary Reports

Professor Albert E. Miller
University of Notre Dame
Box 8
Notre Dame, IN 46556

Professor Karl J. Strnat
University of Dayton
Magnetic Laboratory
Dayton, OH 45469

Dr. J.J. Becker
General Electric Research
and Development Center
P.O. Box 8
Schenectady, NY 12301

Professor W.E. Wallace
Department of Chemistry
University of Pittsburgh
Pittsburgh, PA 15213

Dr. Richard P. Allen
Battelle-Northwest
Richland, WA 99352

Dr. Howard T. Savage
Naval Surface Weapons Center
White Oak
Silver Spring, MD 20910

Mr. Harold Garrett
Air Force Materials Laboratory
LTE, Bldg. 16
Wright-Patterson Air Force Base
Dayton, OH 45433

Dr. L.D. Jennings
Army Materials and Mechanics
Research Center
Watertown, MA 02172

Dr. J.O. Dimmock, Director
Electronic and Solid State
Sciences Program (Code 427)
Office of Naval Research
Arlington, VA 22217

Assistant Chief for Technology
(Code 2000)
Office of Naval Research
Arlington, VA 22217

Strategic Systems Projects Office
Department of the Navy
Washington, DC

Professor G.S. Ansell
Rensselaer Polytechnic Institute
Dept. of Metallurgical Engineering
Troy, NY 12181

Dr. David L. Martin
General Electric Research
and Development Center
P.O. Box 8
Schenectady, NY 12301

Professor M. Cohen
Massachusetts Institute of Technology
Department of Metallurgy
Cambridge, MA 02139

Professor J.W. Morris, Jr.
University of California
College of Engineering
Berkeley, CA 94720

Professor O.D. Sherby
Stanford University
Materials Sciences Division
Stanford, CA 94300

SUPPLEMENTARY DISTRIBUTION LIST (Continued)

Dr. E.A. Starke, Jr.
Georgia Institute of Technology
School of Chemical Engineering
Atlanta, GA 30332

Professor David Turnbull
Harvard University
Division of Engineering and
Applied Physics
Cambridge, MA 02139

Dr. D.P.H. Hasselman
Montana Energy and MHD Research
and Development Institute
P.O. Box 3809
Butte, MT 59701

Dr. L. Hench
University of Florida
Ceramics Division
Gainesville, FL 32601

Dr. J. Ritter
University of Massachusetts
Department of Mechanical
Engineering
Amherst, MA 01002

Professor J.B. Cohen
Northwestern University
Dept. of Material Sciences
Evanston, IL 60201

Director
Materials Sciences
Defense Advanced Research
Projects Agency
1400 Wilson Boulevard
Arlington, VA 22209

Professor H. Conrad
University of Kentucky
Materials Department
Lexington, KY 40506

Dr. A.G. Evans
Dept. of Material Sciences
and Engineering
University of California
Berkeley, CA 94720

Professor H. Herman
State University of New York
Material Sciences Division
Stony Brook, NY 11794

Professor J.P. Hirth
Ohio State University
Metallurgical Engineering
Columbus, OH 43210

Professor R.M. Latanision
Massachusetts Institute of Technology
77 Massachusetts Avenue
Room E19-702
Cambridge, MA 02139

Dr. Jeff Perkins
Naval Postgraduate School
Monterey, CA 93940

Dr. R.P. Wei
Lehigh University
Institute for Fracture and
Solid Mechanics
Bethlehem, PA 18015

Professor G. Sines
University of California
at Los Angeles
Los Angeles, CA 90024

Professor H.G.F. Wilsdorf
University of Virginia
Department of Materials Science
Charlottesville, VA 22903

Dr. A. Tauber
Dept. of the Army
HQ, U.S. Army Electronic Command
Fort Monmouth, NY 07703

SUPPLEMENTARY DISTRIBUTION LIST (Continued)

Mr. K.K. Jin
Strategic Systems Division
Autonetics Group
3370 Miraloma Avenue
P.O. Box 4192
Anaheim, CA 92803

Mr. N. Horowitz
The Aerospace Corporation
2350 East El Segundo Boulevard
El Segundo, CA

Mr. Francis W. Wessbecher
Unit Head
Inertial Component Engineering
Singer Kearfott Division
150 Totowa Road
Wayne, NJ 07470

National Magnet Laboratory
Massachusetts Institute of Technology
145 Albany Street
Cambridge, MA 02139
ATTN: Dr. Donald T. Stevenson (2)
Assistant Director

Mr. Carl Flom
Delco Electronics
7929 South Howell
Box 471
Milwaukee, WI 53201

David Schwab
Air Research Mfg. Co.
2525 W. 190th Street
Torrance, CA 90209

END

DATE
FILMED

5 -83

DTIC